11-16-2003

Chemical and physical properties of bulk aerosols within four sectors observed during TRACE-P

C. Jordan
University of New Hampshire

B E. Anderson
NASA

R. Talbot
University of New Hampshire, robert.talbot@unh.edu

Jack E. Dibb
University of New Hampshire, jack.dibb@unh.edu

H Fuelberg
Florida State University

See next page for additional authors

Recommended Citation

Jordan, C. E., et al. (2003), Chemical and physical properties of bulk aerosols within four sectors observed during TRACE-P, J. Geophys. Res., 108, 8813, doi:10.1029/2002JD003337, D21.

Chemical and physical properties of bulk aerosols within four sectors observed during TRACE-P

C. E. Jordan,[1] B. E. Anderson,[2] R. W. Talbot,[3] J. E. Dibb,[4] H. E. Fuelberg,[5]
C. H. Hudgins,[2] C. M. Kiley,[5] R. Russo,[4] E. Scheuer,[3] G. Seid,[3]
K. L. Thornhill,[6] and E. Winstead[7]

Received 20 December 2002; revised 12 May 2003; accepted 27 May 2003; published 15 November 2003.

[1] Chemical and physical aerosol data collected on the DC-8 during TRACE-P were grouped into four sectors based on back trajectories. The four sectors represent long-range transport from the west (WSW), regional circulation over the western Pacific and Southeast Asia (SE Asia), polluted transport from northern Asia with substantial sea salt at low altitudes (NNW) and a substantial amount of dust (Channel). WSW has generally low mixing ratios at both middle and high altitudes, with the bulk of the aerosol mass due to non-sea-salt water-soluble inorganic species. Low altitude SE Asia also has low mean mixing ratios in general, with the majority of the aerosol mass comprised of non-sea-salts, however, soot is also relatively important in this region. NNW had the highest mean sea salt mixing ratios, with the aerosol mass at low altitudes (<2 km) evenly divided between sea salts, non-sea-salts, and dust. The highest mean mixing ratios of water-soluble ions and soot were observed at the lowest altitudes (<2 km) in the Channel sector. The bulk of the aerosol mass exported from Asia emanates from Channel at both low and midaltitudes, due to the prevalence of dust compared to other sectors. Number densities show enhanced fine particles for Channel and NNW, while their volume distributions are enhanced due to sea salt and dust. Low-altitude Channel exhibits the highest condensation nuclei (CN) number densities along with enhanced scattering coefficients, compared to the other sectors. At midaltitudes (2–7 km), low mean CN number densities coupled with a high proportion of nonvolatile particles ($\geq$65%) observed in polluted sectors (Channel and NNW) are attributed to wet scavenging which removes hygroscopic CN particles. Low single scatter albedo in SE Asia reflects enhanced soot. *INDEX TERMS:* 0305 Atmospheric Composition and Structure: Aerosols and particles (0345, 4801); 0345 Atmospheric Composition and Structure: Pollution—urban and regional (0305); 0365 Atmospheric Composition and Structure: Troposphere—composition and chemistry; 0368 Atmospheric Composition and Structure: Troposphere—constituent transport and chemistry; *KEYWORDS:* aerosols, TRACE-P, Asia

Citation: Jordan, C. E., et al., Chemical and physical properties of bulk aerosols within four sectors observed during TRACE-P, *J. Geophys. Res.*, *108*(D21), 8813, doi:10.1029/2002JD003337, 2003.

1. Introduction

[2] TRACE-P (Transport and Chemical Evolution Over the Pacific was conducted over the western Pacific), just off the coast of Asia, from February to April of 2001. Two aircraft were used to investigate the chemical composition of Asian outflow over the western Pacific and its chemical evolution [*Jacob et al.*, 2003]. Aerosols are an important component of Asian continental outflow. Throughout this special section, aerosols are shown to be important not just in their own right, but also for the interactions which influence gas phase processes as well [*Crawford et al.*, 2003; *Jordan et al.*, 2003; *Lefer et al.*, 2003; *Price et al.*, 2003; *Tang et al.*, 2003a, 2003b].

[3] TRACE-P was conducted in spring for several reasons [*Jacob et al.*, 2003]. This is the season when Asian export to the Pacific is at its maximum, biomass burning peaks during this time in Southeast Asia, photochemistry is already active, and stratospheric intrusions are also at their

[1]National Research Council, NASA Langley Research Center, Hampton, Virginia, USA.
[2]Atmospheric Sciences Competency, NASA Langley Research Center, Hampton, Virginia, USA.
[3]Complex Systems Research Center, Institute for the Study of Earth, Oceans, and Space, University of New Hampshire, Durham, New Hampshire, USA.
[4]Climate Change Research Center, Institute for the Study of Earth, Oceans, and Space, University of New Hampshire, Durham, New Hampshire, USA.
[5]Department of Meteorology, Florida State University, Tallahassee, Florida, USA.
[6]SAIC, NASA Langley Research Center, Hampton, Virginia, USA.
[7]GATS, NASA Langley Research Center, Hampton, Virginia, USA.

0148-0227/03/2002JD003337

maximum. Further, the cold fronts which are responsible for the strong seasonal outflow to the Pacific also give rise to dust storms, making spring the season of maximum dust export as well [*Sun et al.*, 2001; *Jacob et al.*, 2003]. Hence, natural and anthropogenic aerosol emissions, which include dust, biomass-burning particulates, and anthropogenic pollutant aerosols, are anticipated to be at a maximum at this time of year.

[4] A better understanding of aerosols and the processes in which they are involved is needed for a variety of reasons. As discussed by *Streets et al.* [2003], black carbon and organic carbon emissions are the most poorly constrained species in their Asian emission inventories. *Crawford et al.* [2003] report statistically significant differences in trace gas concentrations between clear-sky and cloudy conditions. This has implications for whether satellite retrievals adequately represent the export and evolution of various species in outflow associated with cloudy frontal regions. *Lefer et al.* [2003] and *Tang et al.* [2003a, 2003b] both discuss the influence of clouds and aerosols on photolysis frequencies and hence photochemistry. Better knowledge of aerosol optical properties is needed (e.g., aerosol optical depth and single scatter albedo) to improve measurement/model agreement [*Lefer et al.*, 2003]. Meanwhile, Asian aerosols are found on average to have a greater photochemical influence than clouds during TRACE-P, reducing photolysis rates throughout the column [*Tang et al.*, 2003a].

[5] *Price et al.* [2003] report observations in North America of Asian dust, mixed with pollution, where O_3 and aerosol scatter were anti-correlated. The authors suggest that this may be attributed to either reduced O_3 formation on account of the large amount of dust reducing UV reaching the surface, or the loss of O_3 to the surface of the dust particles. *Jordan et al.* [2003] report evidence of the uptake of NO_3^- and $SO_4^=$ on dust particles, resulting in a change in the phase partitioning of these species with implications for both deposition to the western Pacific coastal waters and chemical evolution of the air mass downwind.

[6] Companion papers in this special section each address specific questions pertaining to the role of aerosols in the chemical composition and evolution of Asian outflow. In this paper we present an overview of the aerosol physical and chemical properties as measured on the DC-8, flights 8–18 (19°–45°N, 115°–198°E). Back trajectories are used to divide the aerosol data into four sectors reflecting the general geographic origins of the particles. The chemical and physical properties of these bulk aerosols are evaluated together to yield a comprehensive picture of the particulates in this region. As is discussed elsewhere, aerosols in this area are highly heterogeneous in their distribution [*Dibb et al.*, 2003; *Ma et al.*, 2003]. However, given the incomplete descriptions of particles presently incorporated into regional and global atmospheric models, and the need for validation of satellite aerosol observations on fairly large geographic scales, we believe this broad description may be useful.

2. Methods

2.1. Aerosol Physical Properties

[7] The suite of instruments flown aboard the DC-8 included: three condensation nuclei counters (CNC) to obtain the number densities and volatility of submicron aerosols; a Passive Cavity Aerosol Spectrometer Probe (PCASP) to measure the dry size of 0.1–3.0 μm diameter particles, a Forward Scattering Spectrometer Probe (FSSP-300) to obtain size spectra of 0.3–20 μm particles under ambient conditions; a 3-wavelength nephelometer (TSI 3560) to measure aerosol scattering coefficients at wavelengths of 450, 550, and 700 nm; and a Particle Soot Absorption Photometer (PSAP) to measure total aerosol absorption, from which the mass of soot particles was determined.

[8] The CNCs drew samples from a common manifold maintained at a constant pressure of either 213 or 267 hPa, depending on flight level, to eliminate altitude-related fluctuations in sensitivity and performance. The CN data have been corrected for the pressure dependent sensitivities of the counters (typically 30 to 40%) and are presented in units of number per cubic centimeter at sea level conditions (20°C and 1013 hPa, STP). These number densities are estimated to have ±20% precision, due primarily to uncertainies in particle loss through the sample inlet and imprecision in the instrument flow rate measurements.

[9] The PCASP and FSSP-300 probes were mounted on a pylon extending 0.5 m below the aircraft's left wing-tip, a location calculated to be minimally affected by aircraft-induced flow distortion. The FSSP-300 has an open sample cavity that provides size distribution measurements at ambient temperature and humidity conditions. PCASP dehydrates aerosols to <30% RH prior to measurement due to sample air being drawn through a heated capillary tube to the resonance cavity, combined with the sample air being surrounded by a concentric flow of dry filtered air to maintain laminar flow through the cavity. The probes' size sensitivities were determined using non-absorbing latex spheres with real and imaginary refractive indices, n_r and n_i, of 1.59 and 0.0, respectively. These data were then used in conjunction with output from a Mie scattering model to set the PCASP and FSSP size-channel thresholds for aerosols with real refractive indices of 1.55 (sulfate) and 1.44 (hydrated sea salt), respectively. Number densities provided by the two instruments are estimated to have a ±25% precision due largely to the difficulty in defining the instruments' effective sample volumes.

[10] Aerosol scattering coefficients (σ_{sp}) were measured at 450, 550, and 700 nm using a TSI model 3563 Integrating Nephelometer [i.e., *Bodhaine et al.*, 1991; *Anderson et al.*, 1996]. This instrument would ideally collect light scattered from its sample volume over a 180° viewing angle, but practical considerations limit its integrating volume to between 7° and 170°. *Anderson et al.* [1996] discuss this truncation problem and calculate that it may cause the instrument to significantly underestimate σ_{sp} for aerosol populations dominated by supermicron sized particles. Because, as discussed below, our sample inlet did not efficiently transmit particles >1 μm in diameter, we have simply applied a truncation error correction factor of 1.07 to the entire scattering coefficient data set.

[11] Aerosol absorption coefficients (σ_{ap}) at 565 nm were measured with a Radiance Research Particle Soot Absorption Photometer (PSAP). These data were corrected for aerosol scattering using the technique proposed by *Bond et al.* [1999] and were filtered to remove time periods when the instrument performed poorly due to rapid changes in

sample pressure and humidity. Even so, this particular instrument was exceptionally noisy when operated at reduced pressures. Thus its data use is limited to establishing a mean single scattering albedo value (ω_o) and inferring soot mass (assuming an absorption efficiency of 10 m^2g^{-1}) in polluted air masses where σ_{ap} exceeded 1 Mm^{-1}.

[12] Sample air for the nephelometer and PSAP were drawn in through a forward facing, knife-edge type inlet probe mounted on a window plate adjacent to the aerosol instrument rack. This probe extended ~30 cm out from the aircraft skin, had a tip diameter of 0.3 cm and a 7° conical expansion region downstream of the tip which gradually expanded the flow out into a 2.5-cm i.d. stainless steel pipe. The pipe was bent at a 60° angle and brought through the window plate where it was connected to the nephelometer using a short length (~0.5 m) of conductive tubing of approximately the same inside diameter. A "tee" was placed in this tubing and used to supply ~2 LPM of flow to the PSAP. The exhaust of the nephelometer was connected to a window-mounted venturi pump across a large diameter ball valve that was adjusted to maintain isokinetic flow at the probe tip. This typically resulted in a volumetric flow of ~100 LPM through the nephelometer. In order to evaluate inlet losses for this probe, we compared σ_{sp} measured by the nephelometer with values calculated from PCASP size distributions truncated at various upper size-diameters. Data collected in the marine boundary layer (MBL), where 50–75% of the overall scattering was due to coarse particles, showed the nephelometer data had the best overall fit with scattering parameters calculated from PCASP size distributions cut off at 1 μm diameter.

[13] To relate "dry" aerosol optical parameters back to ambient conditions we applied humidity corrections using the formula $\sigma_{sp}(RH) = \sigma_{sp}(dry)\ (1 - RH/100)^{-g}$ [*Kasten*, 1969] We selected a value of 0.43 for g to yield a $\sigma_{sp}(80\%)/\sigma_{sp}(30\%)$ ratio of ~1.7, the value recommended by *Charlson et al.* [1992] for polluted air masses. This approach produces infinitely large values of $\sigma_{sp}(RH)$ as RH approaches 100%, which frequently occurs in the vicinity of clouds. We thus restricted our data set to points with corresponding RH values of ≤95%, which corresponds to a maximum $\sigma_{sp}(RH)/\sigma_{sp}(30\%)$ ratio of ~3.6.

2.2. Aerosol Chemical Properties

[14] The aerosol water-soluble inorganic chemical measurements are described in greater detail elsewhere [*Dibb et al.*, 1999, 2000, 2002, 2003], so only a brief synopsis appears here. Air enters an anodized aluminum curved leading edge nozzle centered in a shroud that extends 20 cm forward of the nozzle. This allows for nearly isoaxial sampling throughout the flight [*Dibb et al.*, 2002, references therein]. Once inside the aircraft, air then flows through a Delrin ball valve, followed by a Delrin diffuser, to a 9 cm, 2 micron Millipore Fluoropore Teflon filter in a Delrin holder [*Dibb et al.*, 2002]. Behind the filter is another valve, a mass flowmeter, and a venturi pump. Sampling flow rates were manually adjusted to be isokinetic within 10% along each flight leg [*Dibb et al.*, 2002]. Filters were processed according to procedures described by *Dibb et al.* [1999, 2000]. Inorganic anion and cation mixing ratios were obtained from ion chromatography. Samples were collected only during level flight legs with sampling times ranging from 3–36 minutes with mean and median times of 10 and 8 minutes, respectively. For a complete discussion of the chemical measurements and error analysis, see *Dibb et al.* [2003]. Note that mixing ratios (pptv) were converted to moles or mass per unit volume using standard cubic meters rather than volumetric cubic meters (e.g., μg m^{-3} STP or μmol SCM^{-1}).

2.3. Back Trajectories

[15] The back trajectories are also discussed in greater detail elsewhere [*Fuelberg et al.*, 1996, 1999, 2000, 2003], so again only an overview is given here. Five day back trajectories were calculated using a kinematic model based on global meteorological analyses from the European Centre for Medium-Range Weather Forecasts (ECMWF) [*Fuelberg et al.*, 2003]. ECMWF data were available for 0000, 0600, 1200, and 1800 UTC, at 60 vertical levels with a T319 spherical harmonic triangular truncation, interpolated to a 1° × 1° latitude-longitude horizontal grid [*Fuelberg et al.*, 2003]. For a thorough description of the trajectory model, see *Fuelberg et al.* [1996, 1999, 2000].

2.4. Group Determinations

[16] Of the three data sets used here, the aerosol chemical data had the coarsest resolution, with sample times ranging from 3–36 minutes. Five day back trajectories were calculated every 5 minutes along level flight legs during TRACE-P. Aerosol physical properties had the highest resolution, with 1 minute averages available for most parameters. We wanted to determine whether aerosols from various source regions had characteristic bulk properties, e.g., a strong biomass-burning signal from Southeast Asia with enhanced absorption, or enhanced pollution from northern Asia with enhanced scattering, etc. In order to properly compare data from these disparate sources, all physical data were averaged to the time intervals of the chemical data. The first step was to assess the back trajectory information to sort the chemical data into groups. While there are limitations to the usefulness of back trajectories [*Kahl*, 1993; *Fuelberg et al.*, 2000; *Maloney et al.*, 2001; *Stohl et al.*, 1995; *Stohl*, 1998], they are suitable for classifying this relatively high-resolution data set into broad categories.

[17] Given the length of chemical sample times, there were potentially 1–7 back trajectories available per sample (typically, 2–3 for most samples). Looking at the trajectories, four distinct groups emerged (Figure 1). Trajectories for samples collected above 7 km altitude are shown in the top left panel of Figure 1. Trajectories are shown from northern Asia (NNW) in red, from the west (WSW) in gold, and from Southeast Asia (SE Asia) in blue. In general, these trajectories for samples collected at high altitudes show relatively long range transport, with altitudes generally well above the height of the Tibetan Plateau (Figure 1, bottom left panel). However, the altitude bins are determined by where the sample was collected, not the altitude of the trajectories themselves during their 5 day histories, so some of these trajectories suggest transport from lower altitudes to the measurement height on the aircraft. In contrast to the high altitude trajectories, low altitude trajectories (those for samples collected below 2 km altitude) are shown in the right panels of Figure 1. The top right panel shows the trajectories from above, while the bottom right panel shows

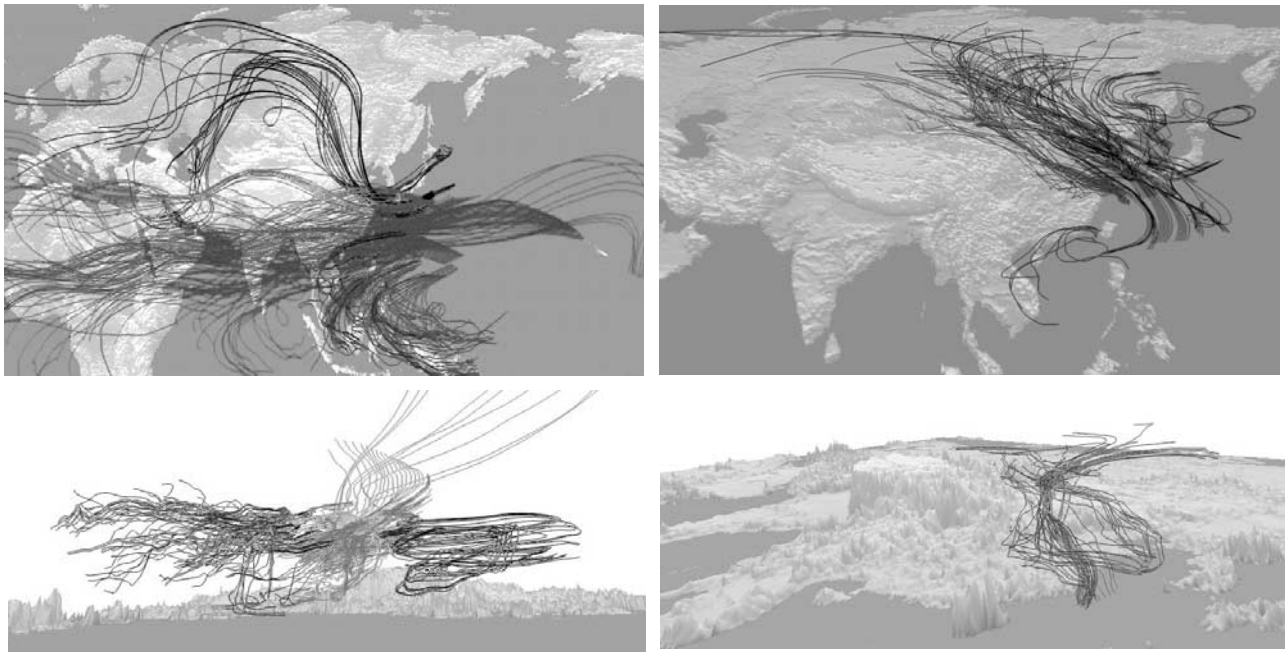

Figure 1. Back trajectories for the aerosol samples divided into four sectors. The top left panel shows trajectories for samples collected at altitudes >7 km. Only three sectors are represented at those altitudes, NNW (red), WSW (gold), and SE Asia (blue). The bottom left panel is a side view from the Pacific Ocean looking toward the Tibetan Plateau. This view shows these trajectories typically represent high altitude long distance transport. The top right panel shows trajectories for samples collected at altitudes <2 km. Only three sectors are represented at these altitudes, NNW (red), Channel (green), and SE Asia (blue). The bottom right panel shows only the low altitude Channel trajectories, angled to show that these trajectories flow along the surface and are confined by the surface topography. See color version of this figure at back of this issue.

an angled view to better show that these low altitude trajectories flow close to the surface and are constrained by its topography. For the low altitude trajectories, red again represents the northern Asia group NNW and blue again represents SE Asia, however, there is an additional group in green called Channel. This can almost be thought of as a subset of the NNW group. However, the chemical data showed greatly enhanced Ca^{2+} in this region, which is what set it apart in this analysis. Midaltitude trajectories (2–7 km, not shown in Figure 1) include all 4 groups, NNW, Channel, WSW, and SE Asia.

[18] Samples with multiple back trajectories were considered "mixed" if the trajectories came from different groups (e.g., a trajectory from SE Asia and another from NNW). Mixed trajectories are due to horizontal and vertical wind shear across the sampling period (distance). Samples were classified as belonging to a particular group only if all trajectories for that sample emanated from the same group. In this way, we evaluated the bulk aerosol properties for each of these four regions with minimal influence from mixed samples. Our deletion of mixed samples insures that geographical partitioning is based only on those trajectory groups with the greatest reliability. Initially, there were 415 chemical samples from 17 flights. Since we are interested in Asian outflow, only samples collected near Asia were included in this analysis (flights 8–18, 19°–45°N, 115°–198°E). Note that only 8 samples (from flight 18) were east of 163°E; the rest were west of 150°E. This left 282 samples. Of these, 70 were mixed, and 19 could not be classified due to missing trajectory data. Mixed trajectories were common during TRACE-P due to numerous middle latitude circulation features that produced shear in the TRACE-P area [*Fuelberg et al.*, 2003]. The remaining samples could be classified into the four groups as follows, 77 NNW, 38 Channel, 47 WSW, and 31 SE Asia.

3. Discussion

3.1. Water-Soluble Ions and Dust

[19] The highest mean water-soluble ion mixing ratios are seen at the lowest altitudes, below 2 km (Figure 2, top panel; Table 1). *Jacob et al.* [2003] attribute this to capping by subsidence inversions at 1–2 km altitude. Channel has the highest concentrations of NH_4^+, $SO_4^=$, and NO_3^- observed (mean mixing ratios of 148, 129, and 108 nmol/m^3, respectively), indicating the highest pollution emanates from this sector. This is not surprising, as the trajectories for this sector pass over many Chinese cities, including Shanghai (Figure 1, top right panel). These elevated aerosol mixing ratios are also consistent with expectations given that Chinese emissions of anthropogenic species dominate those of other Asian regions, contributing 59% of SO_2, 42% of NO_x, 49% of NH_3, 42% of CO, and 41% of black carbon to the total [*Streets et al.*, 2003]. Further, some gas phase species also show enhancements in the Channel sector (Table 2). The highest mean mixing ratios of HNO_3 (1406 pptv), SO_2 (4302 pptv), CO (321 ppbv), and C_2Cl_4 (16 pptv) are found in the low altitude Channel sector

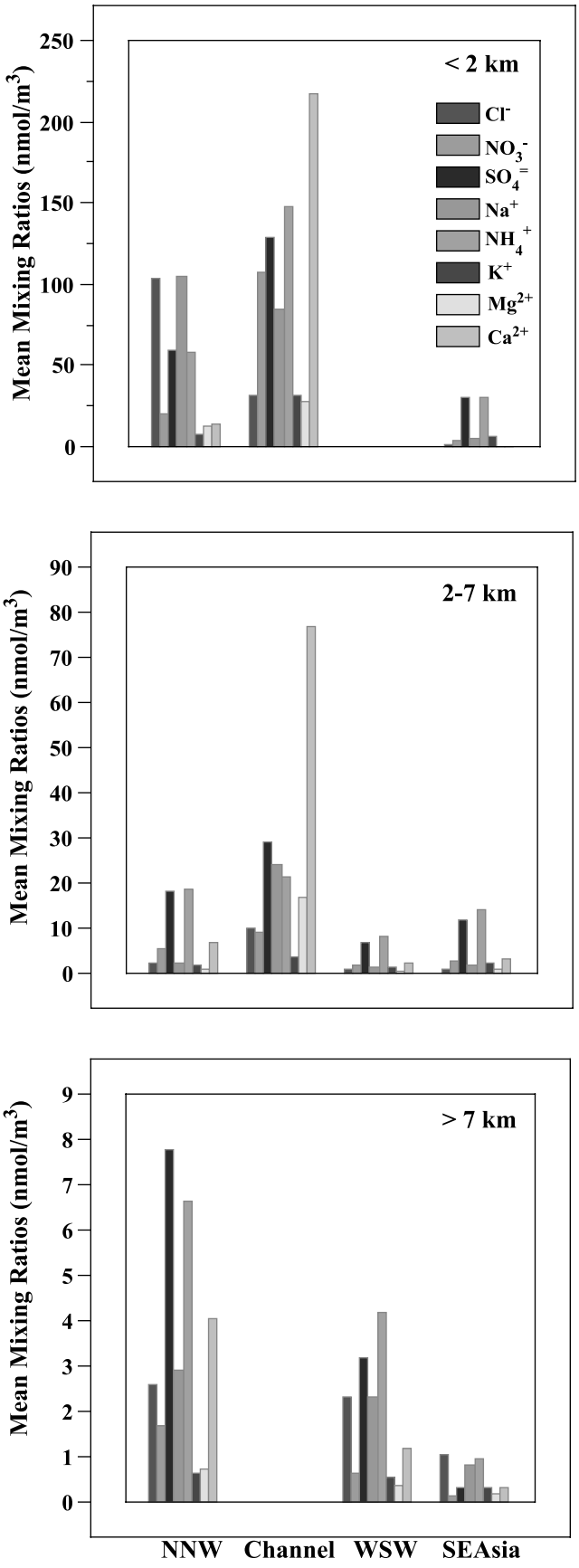

Figure 2. Aerosol mean chemical signatures for each group, split by altitude. See color version of this figure at back of this issue.

(Table 2). This is consistent with the results of *Russo et al.* [2003] and *Talbot et al.* [2003], both of whom used the same sector classification scheme employed here to evaluate trace gas measurements. However, the distinctions observed between aerosols from these sectors are more pronounced than those of the gas phase species [*Russo et al.*, 2003; *Talbot et al.*, 2003]. Note that these enhanced mixing ratios may be compared to background values of 15 pptv (SO_2), 70 ppbv (CO), and 2 pptv (C_2Cl_4) reported by *Russo et al.* [2003]. At midaltitudes, Channel's dominance of mixing ratios does not hold for these gases. This is due to factors other than proximity to sources which control their mixing ratios in the atmosphere, e.g., transport and mixing, photochemical processing, scavenging in clouds, etc.

[20] The striking feature of the Channel group, however, is the dominance of Ca^{2+}, a tracer of dust. The Ca^{2+} mixing ratio is an order of magnitude higher in this group than any other group (e.g., 217 nmol/m^3 versus 14 nmol/m^3 for NNW), which is the case both at low and midaltitudes (Table 1). The Channel trajectories are typical of the transport pathways which carry dust out of the major Asian deserts over the western Pacific [*Sun et al.*, 2001; *Jordan et al.*, 2003]. It is because of the presence of Ca^{2+} in these samples that the Channel group was treated separately from the NNW group. Both NNW and Channel show large amounts of sea salts at low altitudes ($\dot{N}a$ = 105 and 85 nmol/m^3; Cl^- = 104 and 32 nmol/m^3, respectively). The Cl^- deficit (relative to the sea salt ratio) in low altitude Channel samples probably reflects some loss of Cl^- from sea salt due to reaction with acidic gases, but may also be partly an artifact to the extent that some of the measured Na^+ is associated with abundant dust. At these altitudes (<2 km), only two samples had back trajectories classified as SE Asia, and none from WSW. The SE Asia group is much cleaner than the other two groups, nonetheless NH_4^+ and $SO_4^=$ are the dominant water-soluble ions here (31 and 30 nmol/m^3, respectively).

[21] At midaltitudes, NH_4^+ and $SO_4^=$ are the dominant water-soluble ions in aerosols in all groups, except Channel, where dust is still the dominant component as indicated by the dominant Ca^{2+} (77 nmol/m^3), and enhanced Na^+ (24 nmol/m^3) and Mg^{2+} (17 nmol/m^3; Table 1, Figure 2, middle panel). As was the case at low altitude, the highest mixing ratios of the pollution species, NH_4^+ (21 nmol/m^3) and $SO_4^=$ (29 nmol/m^3), are found in the Channel group, followed by NNW (19 and 18 nmol/m^3), SE Asia (14 and 12 nmol/m^3), and WSW (8 and 7 nmol/m^3). High altitude samples (>7 km) have the lowest mixing ratios observed (Figure 2, bottom panel), as expected. NNW shows higher mixing ratios of NH_4^+ (7 nmol/m^3) and $SO_4^=$ (8 nmol/m^3) than the other two groups. Sea salts, $\dot{N}a$ ($\approx$2 nmol/m^3) and Cl^- ($\approx$2 nmol/m^3) are comparable between the three groups (Table 1). Ca^{2+} (4 nmol/m^3) is an important component in the NNW group, but not so much in WSW and SE Asia. Channel is not classified at the highest altitudes, because the high altitude trajectories are sufficiently high as to not be greatly influenced by the defining topography of the Channel group (bounded by the Tibetan Plateau to the south and west, and by mountains to the north). At high altitudes, the Channel and NNW trajectories are combined into the NNW group. While there is dust present in these high altitude samples, it is not dominant, as it is in low and midaltitude

Table 1. Water-Soluble Ion Mixing Ratios and Soot Mass Means, Standard Deviations, Medians, Minima, and Maxima[a]

	Cl^-, nmol/m^3	NO_3^-, nmol/m^3	$SO_4^=$, nmol/m^3	Na^+, nmol/m^3	NH_4^+, nmol/m^3	K^+, nmol/m^3	Mg^{2+}, nmol/m^3	Ca^{2+}, nmol/m^3	Soot, ng/m^3
NNW Sector at <2 km Altitude									
Mean ± SD	103.8 ± 67.0	20.8 ± 13.0	58.9 ± 23.6	105.4 ± 64.4	57.9 ± 22.5	7.8 ± 3.8	12.9 ± 7.2	14.4 ± 12.6	513 ± 224
Median (min.–max.)	102.4 (5.2–252.2)	19.7 (2.1–9.8)	57.1 (11.2–108.5)	105.7 (7.9–255.1)	57.1 (11.6–100.5)	8.2 (0.8–14.0)	12.8 (1.5–27.9)	11.2 (0.6–49.8)	552 (76–897)
No. of samples	41	41	41	41	41	41	41	41	41
NNW Sector at 2–7 km Altitude									
Mean ± SD	2.3 ± 4.4	5.5 ± 17.2	18.3 ± 14.4	2.3 ± 4.1	18.5 ± 17.9	1.8 ± 3.5	1.0 ± 2.0	6.8 ± 11.9	136 ± 164
Median (min.–max.)	1.1 (0.5–22.2)	2.0 (0.4–89.7)	14.5 (2.9–62.1)	0.9 (0.4–16.1)	14.4 (2.7–101.0)	1.1 (0.04–18.5)	0.4 (0.04–9.9)	3.3 (0.04–59.8)	94 (7–837)
No. of samples	26	26	26	26	26	26	26	26	25
NNW Sector at >7 km Altitude									
Mean ± SD	2.6 ± 2.7	1.7 ± 1.1	7.8 ± 3.4	2.9 ± 3.5	6.6 ± 3.5	0.7 ± 0.6	0.7 ± 0.8	4.0 ± 4.9	22 ± 12
Median (min.–max.)	1.4 (0.7–9.1)	1.7 (0.1–3.4)	7.0 (4.0–15.4)	1.2 (0.5–10.4)	7.0 (1.1–13.8)	0.4 (0.2–2.0)	0.3 (0.1–2.1)	1.9 (0.1–13.1)	22 (6–42)
No. of samples	10	10	10	10	10	10	10	10	8
Channel Sector at <2 km Altitude									
Mean ± SD	32.2 ± 24.2	107.7 ± 123.0	129.0 ± 101.1	85.0 ± 101.3	147.5 ± 120.7	31.1 ± 22.8	27.6 ± 26.9	216.9 ± 193.4	2201 ± 1874
Median (min.–max.)	23.5 (11.0–89.5)	45.0 (29.1–602.4)	81.4 (51.7–504.8)	33.0 (16.1–313.7)	96.9 (27.2–639.0)	18.2 (10.4–111.1)	14.3 (1.9–92.8)	138.8 (57.5–629.2)	1199 (1024–9487)
No. of samples	25	25	25	25	25	25	25	25	25
Channel Sector at 2–7 km Altitude									
Mean ± SD	9.9 ± 16.9	8.9 ± 6.7	29.2 ± 26.1	23.9 ± 45.8	21.3 ± 14.7	3.5 ± 3.2	17.0 ± 29.0	76.7 ± 97.9	254 ± 158
Median (min.–max.)	4.4 (0.7–63.5)	7.2 (0.7–23.3)	21.9 (5.5–91.7)	9.5 (0.6–171.6)	14.6 (5.6–47.2)	2.0 (0.1–10.0)	6.9 (0.2–110.0)	34.2 (1.8–329.3)	249 (11–496)
No. of samples	13	13	13	13	13	13	13	13	12
WSW Sector at 2–7 km Altitude									
Mean ± SD	1.1 ± 0.8	1.7 ± 1.7	6.8 ± 4.9	1.6 ± 2.0	8.0 ± 5.1	1.3 ± 0.7	0.5 ± 0.7	2.3 ± 3.5	70 ± 55
Median (min.–max.)	0.8 (0.4–2.8)	1.3 (0.1–5.3)	4.4 (1.5–13.5)	0.7 (0.3–5.9)	5.3 (2.4–16.3)	1.3 (0.3–2.1)	0.2 (0.1–1.8)	0.7 (0.1–10.0)	42 (30–168)
No. of samples	7	7	7	7	7	7	7	7	6
WSW Sector at >7 km Altitude									
Mean ± SD	2.3 ± 3.0	0.6 ± 0.8	3.2 ± 3.4	2.3 ± 3.6	4.2 ± 3.9	0.5 ± 0.5	0.4 ± 0.4	1.2 ± 2.0	38 ± 30
Median (min.–max.)	1.2 (0.8–12.9)	0.3 (0.1–3.5)	2.3 (0.1–13.1)	1.0 (0.6–14.9)	2.6 (0.8–16.9)	0.4 (0.04–2.5)	0.2 (0.1–1.8)	0.3 (0.1–11.1)	31 (1–103)
No. of samples	40	40	40	40	40	40	40	40	31
SE Asia Sector at <2 km Altitude									
Mean ± SD	0.75 ± 0.02	4.3 ± 0.4	29.8 ± 3.1	5.6 ± 1.5	30.8 ± 0.6	6.3 ± 0.3	0.6 ± 0.1	0.5 ± 0.6	638 ± 28
Median (min.–max.)	0.75 (0.73–0.76)	4.3 (4.1–4.6)	29.8 (27.6–31.9)	5.6 (4.5–6.6)	30.8 (30.4–31.3)	6.3 (6.1–6.5)	0.6 (0.5–0.7)	0.5 (0.1–0.9)	638 (618–657)
No. of samples	2	2	2	2	2	2	2	2	2
SE Asia Sector at 2–7 km Altitude									
Mean ± SD	0.9 ± 0.3	2.6 ± 4.1	12.0 ± 9.6	1.9 ± 2.3	14.2 ± 11.5	2.2 ± 1.8	0.9 ± 1.3	3.2 ± 4.5	219 ± 174
Median (min.–max.)	0.9 (0.4–1.4)	1.0 (0.04–13.4)	11.5 (1.7–32.1)	0.8 (0.3–7.0)	14.0 (1.8–38.0)	2.1 (0.2–5.4)	0.3 (0.1–4.1)	1.5 (0.1–13.3)	210 (17–535)
No. of samples	10	10	10	10	10	10	10	10	10
SE Asia Sector at >7 km Altitude									
Mean ± SD	1.0 ± 0.4	0.1 ± 0.1	0.3 ± 1.0	0.8 ± 0.3	0.9 ± 0.7	0.3 ± 0.2	0.2 ± 0.1	0.3 ± 0.4	17 ± 13
Median (min.–max.)	0.9 (0.5–1.8)	0.1 (0.05–0.4)	0.1 (0.04–4.2)	0.7 (0.4–1.4)	0.9 (0.1–2.5)	0.3 (0.04–0.7)	0.2 (0.1–0.3)	0.2 (0.1–1.9)	16 (3–36)
No. of samples	19	19	19	19	19	19	19	19	8

[a]No samples from the Channel sector at >7 km altitude or the WSW sector at <2 km altitude.

Table 2. Mixing Ratios of Various Gases, Means, Standard Deviations, Medians, Minima, Maxima, and Number of Samples[a]

	O_3, ppbv	CO, ppbv	HNO_3, pptv	SO_2, pptv	C_2Cl_4, pptv	HCN, pptv	CH_3Cl, pptv	CH_3CN, pptv
NNW Sector at <2 km Altitude								
Mean ± SD	56 ± 7	204 ± 23	481 ± 213	568 ± 575	12 ± 3	210 ± 40	556 ± 17	99 ± 47
Median (min.–max.)	54 (36–67)	209 (139–249)	434 (78–1010)	321 (38–2300)	11 (6–22)	205 (107–294)	554 (524–589)	84 (69–317)
No. of samples	41	41	41	35	39	27	39	27
NNW Sector at 2–7 km Altitude								
Mean ± SD	58 ± 5	149 ± 50	184 ± 218	600 ± 1158	8 ± 3	229 ± 70	554 ± 19	108 ± 24
Median (min.–max.)	58 (52–66)	126 (109–266)	121 (80–1184)	47 (18–3890)	6 (4–15)	215 (124–354)	548 (528–598)	107 (69–149)
No. of samples	26	26	25	21	26	22	26	22
NNW Sector at >7 km Altitude								
Mean ± SD	131 ± 107	128 ± 49	407 ± 446	103 ± 96	6 ± 4	229 ± 37	542 ± 26	143 ± 43
Median (min.–max.)	75 (54–377)	133 (43–199)	141 (64–1376)	65 (19–257)	6 (1–10)	236 (180–264)	545 (489–578)	126 (95–209)
No. of samples	10	10	10	6	10	4	10	10
Channel Sector at <2 km Altitude								
Mean ± SD	67 ± 10	321 ± 129	1406 ± 1155	4302 ± 3950	16 ± 14	517 ± 340	637 ± 188	144 ± 70
Median (min.–max.)	64 (55–108)	267 (177–830)	910 (597–5914)	2649 (876–20861)	12 (9–79)	319 (259–1612)	559 (540–1458)	106 (80–317)
No. of samples	25	25	25	25	25	21	25	17
Channel Sector at 2–7 km Altitude								
Mean ± SD	59 ± 6	136 ± 25	206 ± 68	137 ± 172	6 ± 2	177 ± 7	562 ± 17	141 ± 45
Median (min.–max.)	57 (48–71)	130 (109–178)	180 (140–346)	94 (19–541)	6 (5–11)	177 (172–188)	555 (543–595)	144 (84–223)
No. of samples	13	13	13	8	13	5	13	11
WSW Sector at 2–7 km Altitude								
Mean ± SD	62 ± 4	118 ± 23	175 ± 47		4 ± 2	271 ± 18	574 ± 26	169 ± 21
Median (min.–max.)	63 (54–66)	112 (95–158)	159 (128–254)		4 (2–8)	270 (241–301)	570 (550–623)	172 (134–199)
No. of samples	7	7	6	0	7	7	7	7
WSW Sector at >7 km Altitude								
Mean ± SD	88 ± 63	134 ± 54	137 ± 114	59	3 ± 2	220 ± 18	589 ± 39	208 ± 57
Median (min.–max.)	76 (35–359)	121 (41–239)	111 (47–670)	59	3 (0.2–7)	213 (205–258)	588 (486–658)	207 (115–305)
No. of samples	40	40	37	1	40	11	40	35
SE Asia Sector at <2 km Altitude								
Mean ± SD	40 ± 1	212 ± 10	793 ± 25		5 ± 0.03	358	634 ± 15	251
Median (min.–max.)	40 (40–41)	212 (205–219)	793 (776–811)		5 (5–5)	358	634 (624–645)	251
No. of samples	2	2	2	0	2	1	2	1
SE Asia Sector at 2–7 km Altitude								
Mean ± SD	51 ± 13	156 ± 81	397 ± 390	154 ± 226	5 ± 4	235 ± 67	591 ± 45	148 ± 35
Median (min.–max.)	54 (29–67)	129 (75–302)	250 (191–1352)	24 (22–415)	4 (2–13)	237 (154–312)	574 (538–674)	135 (126–227)
No. of samples	10	10	8	3	10	6	10	7
SE Asia Sector at >7 km Altitude								
Mean ± SD	34 ± 12	103 ± 32	60 ± 34		3 ± 1	207 ± 76	571 ± 37	152 ± 37
Median (min.–max.)	32 (21–62)	97 (71–191)	50 (26–153)		2 (2–5)	187 (131–344)	556 (531–636)	158 (106–214)
No. of samples	19	19	16	0	19	6	19	16

[a]No samples from the Channel sector at >7 km altitude or the WSW sector at <2 km altitude.

Channel. SE Asia shows the lowest mixing ratios among the high altitude groups (Figure 2, bottom panel). This is not surprising, since these trajectories generally start (5 days earlier) over the Pacific, then carry air over Southeast Asia (Figure 1, top panels).

3.2. Soot

[22] The highest mean soot mass is found in the Channel sector at both low and midaltitudes (2201 and 254 ng/m^3, respectively), followed by SE Asia (638 and 219 ng/m^3, respectively; Figure 3, Table 1). Given the water-soluble chemical data, where NH_4^+ and $SO_4^=$ were much lower in SE Asia than in both Channel and NNW, these soot averages suggest the source of the soot in SE Asia is biomass burning, whereas that in Channel is likely related to residential (biofuel) and industrial sources. HCN, CH_3CN, and CH_3Cl have all been discussed as tracers for biomass burning in other papers in this special section [*Blake et al.*, 2003; *Crawford et al.*, 2003; *Heald et al.*, 2003; *Li et al.*, 2003; *Singh et al.*, 2003]. Here we see that all three of these tracers are elevated in the low altitude Channel samples compared to those from NNW (Table 2). They are also elevated in SE Asia compared to NNW (Table 2). This is consistent with the elevated soot observed here. It seems reasonable to expect that the soot in Channel is due to industrial and residential (biofuels) combustion, while that from SE Asia is due to open biomass burning. However, there does not appear to be a tracer which clearly distinguishes between biofuel and biomass combustion from this analysis.

[23] The high soot observed in Channel and SE Asia is consistent with expected emissions. *Streets et al.* [2003]

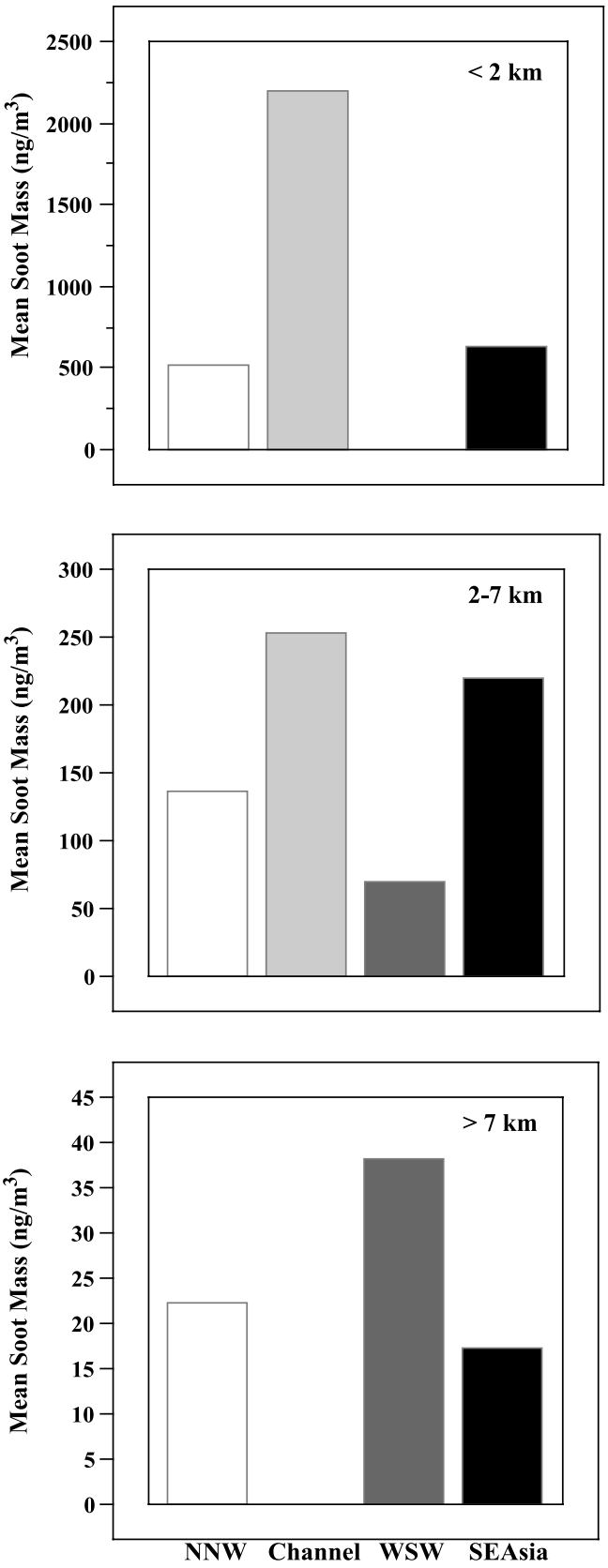

Figure 3. Mean soot mass (ng/m^3) for each group, split by altitude.

estimate that 64% of black carbon emissions are residential and related to the combustion of coal, kerosene, and biofuels in stoves, cookers, and heaters. Most of the rest (18%) is expected to be from biomass burning (which they distinguish from biofuel combustion as open biomass burning, i.e., forest burning, savanna/grassland burning, and crop residues burned in field after harvest). They note that the 18% contribution from biomass burning is primarily due to contributions from Southeast Asia. Further, other studies in this special section also report significant biomass burning from this region [*Heald et al.*, 2003; *Ma et al.*, 2003; *Russo et al.*, 2003; *Tang et al.*, 2003b]. *Liu et al.* [2003] note that deep convection is the most important transport mechanism exporting biomass-burning effluents from Southeast Asia. This is consistent with most of our samples in this sector being collected above 7 km (19 samples) with only 2 samples below 2 km, and the remainder (10 samples) obtained between 2 and 7 km (Table 1). However, it should also be noted, that soot was found in only 8 of the highest altitude samples from SE Asia, and on average these samples generally had an order of magnitude less soot than that found at lower altitudes (Table 1).

[24] Note, even though the water-soluble ion mixing ratios and soot mass were measured with very different techniques, by two different groups, the measurements are consistent with each other as shown in Figure 4. There are very good correlations between soot and both NH_4^+ (R^2 = 0.92) and $SO_4^=$ (R^2 = 0.91), which likely represents similar pollution sources (since SO_2 is typically released by fossil fuel rather than biomass combustion [*Ma et al.*, 2003]). There is no correlation between Na^+ and soot (R^2 = 0.29), which is expected since sea salt and soot aerosols are generated by very different mechanisms. There is a moderate correlation between nss-Ca^{2+} and soot (R^2 = 0.63). However, this is probably coincidental due to the co-location of dust and pollution sources, and hence does not represent a real relationship between processes which emit dust and soot. Finally, the best correlation is found with K^+ (R^2 = 0.96, Figure 4). This is particularly encouraging, since K^+ is predominantly produced by biomass combustion (both open biomass-burning and biofuel combustion) and since K^+ primarily resides in fine mode particles, as does soot [*Ma et al.*, 2003; *Hasegawa and Ohta*, 2002]. This gives us some confidence that the soot mass and water-soluble ion mixing ratios can reasonably be compared.

3.3. Partitioning Between Aerosol Types

[25] To get a better understanding of the partitioning between various aerosol types, the measured constituent masses were calculated and added up for each sample. Then the contribution of each type of aerosol to the total was determined (Table 3). Na^+ was used as the reference species to determine the proportion of sea salts present (Ca^{2+}, Mg^{2+}, K^+, Cl^-, and $SO_4^=$ all have sea salt components). The difference between the total measured water-soluble ions and their sea salt contributions, was used to determine the non-sea-salt fractions (dominated by anthropogenic ammonium sulfate). Using Na^+ as the reference species requires all of the Na^+ to be assigned to the sea salt fraction, even though some is actually due to dust. This results in an overestimate of the sea salt fraction, and an underestimate of

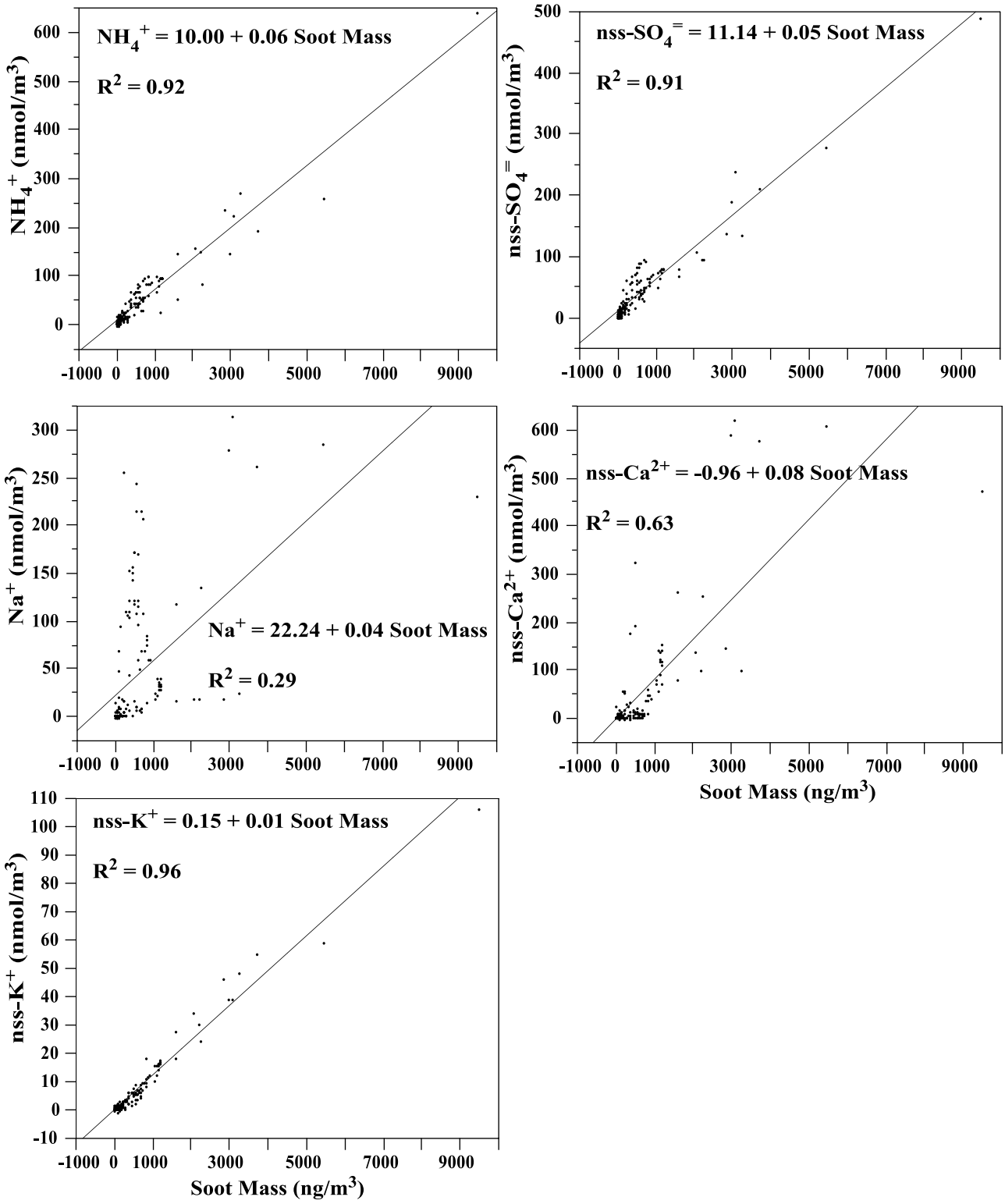

Figure 4. Various water-soluble aerosol species plotted versus soot.

the non-sea-salt fraction. Non-sea-salt-Ca^{2+} (nss-Ca^{2+}) was used to calculate the dust mass, assuming it represents 6.80% of the dust mass by weight [*Song and Carmichael*, 2001]. Since nss-Ca^{2+} is underestimated somewhat due to the problems with using Na^+ as a reference species, the dust fraction is underestimated here somewhat. Note, dust fractions (which include both nss-Ca^{2+} and nss-Mg^{2+}) were not included in the non-sea-salt (NSS) fraction (i.e., NSS = NO_3^- + nss-$SO_4^=$ + NH_4^+ + nss-K^+). Nss-K^+ is primarily produced by combustion processes as discussed in the previous section, however it is also a constituent of Asian dust (0.91% by weight [*Song and Carmichael*, 2001]). Hence, the NSS fraction does represent some dust, particularly in Channel, via the inclusion of all of the nss-K^+.

Table 3. Calculated Aerosol Mass and Percentages Contributing to the Total, Means, Standard Deviations, Medians, Minima, and Maxima[a]

	Total Mass	Soot	SS	NSS	Dust
		NNW Sector at <2 km Altitude			
Mean ± SD	22.6 ± 10.8	2.5 ± 1.5	33.2 ± 19.2	36.4 ± 10.1	27.8 ± 19.0
Median (min.–max.)	20.7 (4.8–46.4)	2.0 (0.5–7.0)	34.9 (4.1–77.1)	35.1 (19.3–63.8)	27.7 (0–63.9)
No. of samples	41	41	41	41	41
		NNW Sector at 2–7 km Altitude			
Mean ± SD	6.9 ± 9.7	2.2 ± 1.8	2.4 ± 2.0	50.7 ± 23.2	44.7 ± 24.3
Median (min.–max.)	3.9 (0.4–50.5)	1.6 (0–8.2)	1.6 (0.4–7.3)	46.0 (16.6–90.8)	50.9 (2.0–79.8)
No. of samples	26	26	26	26	26
		NNW Sector at >7 km Altitude			
Mean ± SD	3.6 ± 3.4	0.8 ± 0.7	5.5 ± 3.1	49.6 ± 27.9	44.1 ± 29.6
Median (min.–max.)	2.1 (0.7–10.4)	0.6 (0–1.8)	5.1 (1.5–11.7)	46.6 (15.9–85.3)	50.3 (7.7–78.6)
No. of samples	10	10	10	10	10
		Channel Sector at <2 km Altitude			
Mean ± SD	133.8 ± 112.1	1.7 ± 0.7	2.3 ± 0.7	17.4 ± 7.3	78.6 ± 7.5
Median (min.–max.)	97.3 (46.1–422.1)	1.5 (0.7–3.2)	2.4 (0.9–3.5)	15.8 (6.9–36.4)	80.4 (58.7–89.1)
No. of samples	23	23	23	23	23
		Channel Sector at 2–7 km Altitude			
Mean ± SD	50.1 ± 62.0	0.8 ± 0.7	2.1 ± 1.1	15.2 ± 11.7	81.9 ± 11.8
Median (min.–max.)	25.1 (1.8–210.2)	0.6 (0–2.4)	1.9 (0.6–3.8)	9.2 (4.7–38.4)	87.3 (58.7–92.4)
No. of samples	13	13	13	13	13
		WSW Sector at 2–7 km Altitude			
Mean ± SD	2.5 ± 2.7	4.3 ± 3.9	6.4 ± 7.7	53.4 ± 18.9	35.9 ± 24.4
Median (min.–max.)	1.9 (0.5–8.1)	5.0 (0–9.1)	3.7 (1.1–2.3)	57.3 (23.5–75.7)	33.9 (10.1–72.4)
No. of samples	7	7	7	7	7
		WSW Sector at >7 km Altitude			
Mean ± SD	1.3 ± 1.4	3.9 ± 4.4	14.0 ± 12.3	45.6 ± 25.0	36.5 ± 28.2
Median (min.–max.)	0.8 (0.2–7.9)	2.3 (0–15.1)	11.3 (1.8–54.8)	49.7 (5.2–88.0)	25.0 (0–90.3)
No. of samples	40	40	40	40	40
		SE Asia Sector at <2 km Altitude			
Mean ± SD	5.3 ± 0.6	12.2 ± 2.0	3.9 ± 0.5	79.8 ± 4.2	4.1 ± 5.7
Median (min.–max.)	5.3 (4.8–5.7)	12.2 (10.8–13.6)	3.9 (3.6–4.3)	79.8 (76.8–82.8)	4.1 (0.04–8.1)
No. of samples	2	2	2	2	2
		SE Asia Sector at 2–7 km Altitude			
Mean ± SD	3.9 ± 4.2	7.4 ± 4.8	3.3 ± 1.8	53.8 ± 20.4	35.5 ± 24.4
Median (min.–max.)	2.5 (0.4–13.6)	7.0 (1.4–16.2)	2.7 (1.3–7.5)	52.6 (19.1–80.5)	36.0 (4.4–76.6)
No. of samples	10	10	10	10	10
		SE Asia Sector at >7 km Altitude			
Mean ± SD	0.3 ± 0.3	4.1 ± 6.9	23.4 ± 10.3	27.1 ± 16.1	45.5 ± 22.3
Median (min.–max.)	0.2 (0.1–1.2)	0 (0–20.4)	26.7 (4.3–35.5)	26.6 (3.9–76.3)	39.4 (12.7–91.7)
No. of samples	17	17	17	17	17

[a]Total mass is in units of $\mu g/m^3$. All other numbers are percentages. No samples from the Channel sector at >7 km altitude or the WSW sector at <2 km altitude.

Also note, organic species are not included in this discussion. This may be a significant factor, especially for SE Asia where biomass-burning sources may result in organic particulates which constitute a substantial fraction of the mass (e.g., *Mayol-Bracero et al.* [2002] reported that particulate organic matter constituted 35% of the fine aerosol mass during the Indian Ocean Experiment (INDOEX)).

[26] The bulk of the aerosol mass exported from Asia is carried in the Channel sector, 134 $\mu g/m^3$ on average below 2 km (Table 3). This is almost a factor of 6 higher than that from the NNW sector at the same altitudes. At midaltitudes Channel still carries the most material, 50 $\mu g/m^3$ on average between 2 and 7 km, about a factor of 7 higher than that of NNW. At midaltitudes, SE Asia and WSW contain only about half the material present in NNW. At high altitudes, NNW contains only about half the material that was present there at midaltitudes, 3.6 $\mu g/m^3$ on average, which is about 3 times that in WSW and 10 times that in SE Asia.

[27] At low altitudes, only about 2% of the aerosol mass in Channel is due to either soot or sea salt. 17% is NSS, while the remaining 79% of the mass in Channel is dust (Table 3). The percentages are similar for midaltitude Channel samples with dust increasing to 82%, NSS dropping to 15%, and soot dropping to 1%. NNW also has a low percentage of soot (3%), but the sea salt, NSS, and dust fractions are all comparable at low altitudes, at 33%, 36%, and 28%, respectively. At midaltitudes, the sea salts are far less important, contributing only 2% to the total mass in NNW, resulting in NSS constituting 51% and dust 45% of

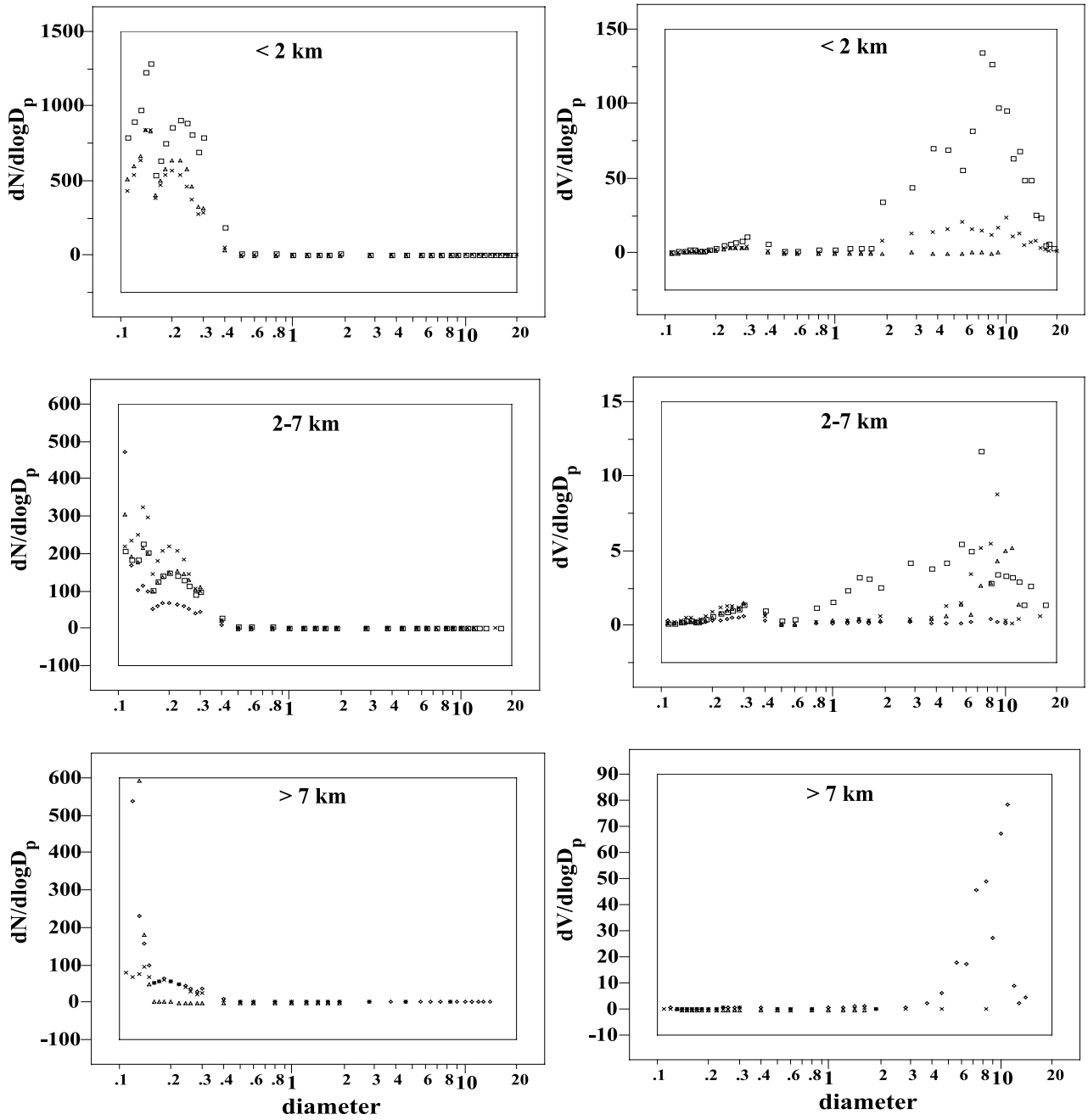

Figure 5. Size distributions of particle number (left panels) and dry particle volume (right panels) are shown for particle sizes ranging from 0.11–20 μm diameter. These distributions are binned according to altitude (separate panels) and groups (NNW (x's), Channel (squares), WSW (circles), and SE Asia (triangles)).

the mass, while soot remains at 2%. These percentages remain nearly the same for high altitude NNW.

[28] SE Asia particulate mass, on the other hand, is about 12% soot, with sea salts and dust each only adding 4%, while the bulk of material, 80% is NSS at low altitude. At midaltitude, soot comprises 7% of the mass, while sea salt remains low at about 3%, and NSS drops to 54% due to the relative increase in dust to 36%. At high altitudes, soot comprises 4%, while sea salt and NSS are comparable at 23% and 27%, respectively, and dust increases to 46%. Note, there is very little mass here, compared with the other altitudes and groups, and there is wide variability in these high altitude SE Asia fractions.

[29] WSW has about 4% soot and 36% dust at both middle and high altitudes, while sea salt contributes 6% and 14%, respectively, and NSS makes up the rest at 53% and 46%.

[30] As pointed out by *Jacob et al.* [2003], only minor dust plumes were sampled during TRACE-P. The largest dust plumes in 2001 appeared after TRACE-P and were sampled by ACE-Asia and PHOBEA-II [*Jacob et al.*, 2003; *Huebert et al.*, 2003; *Price et al.*, 2003]. This suggests that

dust export from a major storm event, and any associated pollution, may substantially exceed the mass presented here.

3.4. Size Distributions

[31] Number densities (Figure 5, left panels) show the highest concentrations in the fine mode occur in the low altitude Channel samples. Note that the instrument response drops off for the smallest sizes. It is expected, that rather than peaking at about 0.14 μm, the number densities should increase all the way down to 0.11 μm, the smallest particle diameter shown here. There is a secondary peak around 0.22 μm diameter present at all altitudes. The high values seen in the Channel number densities support the chemical data in that pollution is highest in this sector. However, at midaltitudes, the highest number densities are generally in the NNW sector, except for the high values seen in WSW and SE Asia. This also supports the chemical data, where the highest pollution species mixing ratios were seen in Channel and NNW. For the most part, number densities decrease with altitude. However, some high values are in SE Asia and WSW in the highest altitude samples.

[32] Volume distributions (Figure 5, right panels) show the highest volumes in the Channel sector at low altitudes. The high volumes seen in the supermicron sizes for both Channel and NNW are due to both dust and sea salts. This is still the case at midaltitudes, but the volumes are about an order of magnitude smaller. Note, a small enhancement in volume is seen at all altitudes around 0.3 μm, which is likely due to the high number of accumulation mode particles. Some fraction of these are likely the $(NH_4)_2SO_4$ (or NH_4HSO_4) seen in the chemical data. These size distributions, both number and volume, have excluded samples collected when the DC-8 flew through a cloud. This led to the exclusion of 11 NNW (5 low, 2 middle, 4 high altitude), 0 Channel, 6 WSW (1 middle, 5 high altitude), and 5 SE Asia (2 middle, 3 high altitude) samples. Had the cloud data remained, the volume curves were seen to increase dramatically from 5–20 μm. For the most part, the influence of cloud data has been removed. However, at high altitudes, the high volumes seen in WSW supermicron volumes is likely due to passage near a cloud, with some residual enhanced particle volumes (Figure 5, bottom right panel).

[33] The low altitude size distributions here are consistent with those from various marine boundary layer locations reported by *Bates et al.* [2002]. They showed number distributions had a peak at 0.2 μm from many source regions measured during INDOEX, Aerosols99, ACE-1, and ACE-2. Some of these locations also exhibited number density peaks at sub-0.1 μm diameters, while others did not. A volume distribution curve from the Atlantic Ocean of African mineral dust exhibited the highest volume in their comparison with a peak $dV/dlogD_p$ value of about 70 for 2.5 μm particles, compared to about 125 for 8 μm particles here.

3.5. Condensation Nuclei

[34] Mean condensation nuclei measurements (Figure 6 and Table 4) are again highest in the low altitude Channel sector (17084 cm^{-3} CN > 4 nm, 12182 cm^{-3} CN > 14 nm). Number densities of mean condensation nuclei >4 nm (#/cm^3 at STP) are shown along with unheated and heated measurements of CN > 14 nm (Figure 6 and Table 4). The

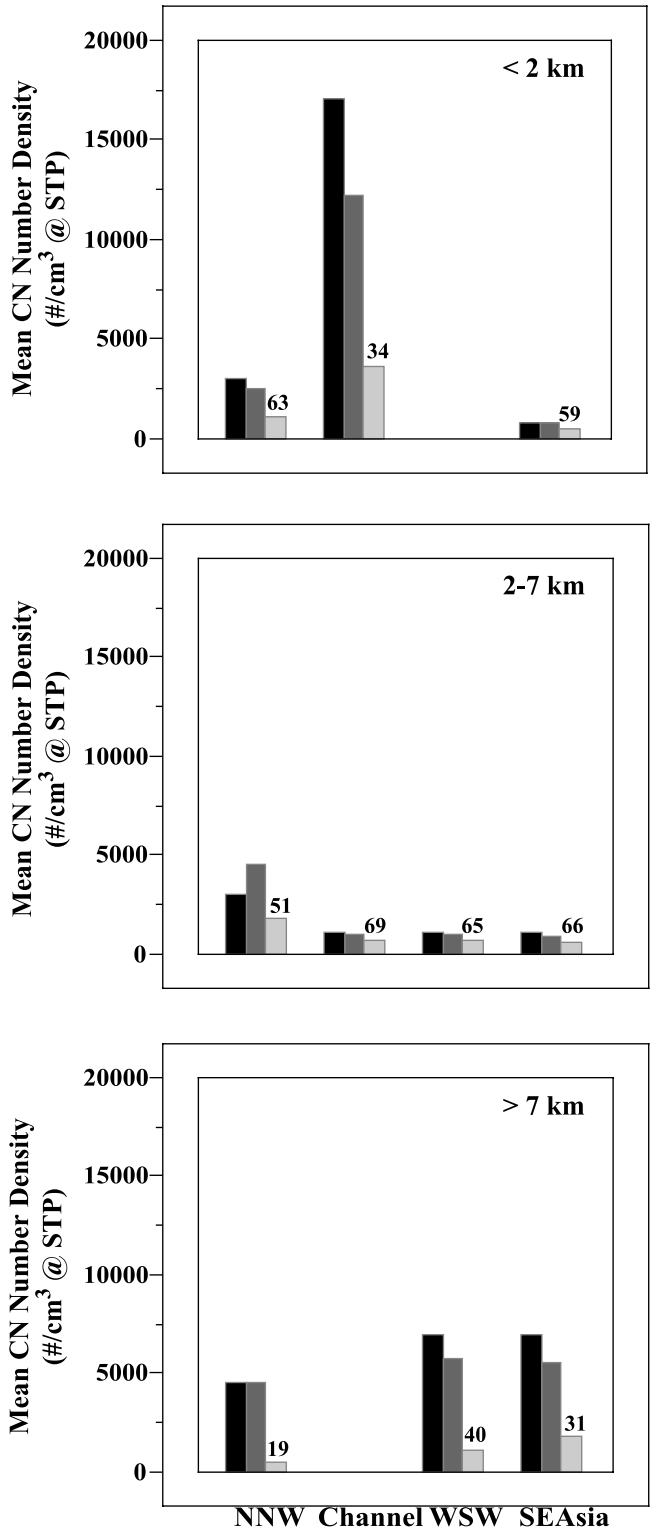

Figure 6. Mean condensation nuclei (CN) > 4 nm (black), unheated CN > 14 nm (medium gray), and heated CN > 14 nm (light gray), split by group and altitude. The numbers above the heated CN columns are the percentages of the total for each group represented by nonvolatile CN > 14 nm.

Table 4. Condensation Nuclei and Volatility, Means, Standard Deviations, Medians, Minima, Maxima, and Number of Samples[a]

		CN > 14 nm		
	CN > 4 nm	Unheated	Heated	Ratio (Heated/Unheated)
		NNW Sector at <2 km Altitude		
Mean ± SD	2988 ± 4901	2520 ± 3495	1107 ± 919	0.63 ± 0.27
Median (min.–max.)	1111 (36–23274)	1068 (38–16611)	686 (16–3765)	0.70 (0.04–0.99)
No. of samples	38	41	39	39
		NNW Sector at 2–7 km Altitude		
Mean ± SD	3073 ± 3327	4553 ± 11084	1851 ± 1356	0.51 ± 0.32
Median (min.–max.)	1202 (371–9625)	767 (433–49923)	1661 (289–4537)	0.41 (0.10–0.97)
No. of samples	26	20	8	8
		NNW Sector at >7 km Altitude		
Mean ± SD	4595 ± 8685	4508 ± 7898	457 ± 311	0.19 ± 0.19
Median (min.–max.)	1654 (686–29120)	1479 (547–26096)	363 (8–915)	0.13 (0.004–0.43)
No. of samples	10	10	7	7
		Channel Sector at <2 km Altitude		
Mean ± SD	17084 ± 18087	12182 ± 12604	3645 ± 3313	0.34 ± 0.27
Median (min.–max.)	10683 (1018–70675)	4811 (1062–40746)	2445 (765–11718)	0.26 (0.03–0.82)
No. of samples	23	20	10	10
		Channel Sector at 2–7 km Altitude		
Mean ± SD	1100 ± 873	1041 ± 814	696 ± 444	0.69 ± 0.18
Median (min.–max.)	675 (405–3418)	631 (378–3132)	512 (321–1871)	0.61 (0.50–1.03)
No. of samples	13	13	13	13
		WSW Sector at 2–7 km Altitude		
Mean ± SD	1132 ± 366	1023 ± 311	666 ± 106	0.65 ± 0.21
Median (min.–max.)	1064 (730–1762)	998 (685–1563)	672 (481–796)	0.63 (0.31–0.92)
No. of samples	7	7	7	7
		WSW Sector at >7 km Altitude		
Mean ± SD	6963 ± 12334	5778 ± 9906	1104 ± 932	0.40 ± 0.21
Median (min.–max.)	2150 (594 –50592)	1993 (583–42289)	913 (214–4678)	0.37 (0.02–0.89)
No. of samples	40	40	38	38
		SE Asia Sector at <2 km Altitude		
Mean ± SD	815 ± 30	829 ± 34	513 ± 30	0.59 ± 0.06
Median (min.–max.)	815 (794–837)	829 (805–853)	513 (492–535)	0.59 (0.55–0.63)
No. of samples	2	2	2	2
		SE Asia Sector at 2–7 km Altitude		
Mean ± SD	1127 ± 1017	928 ± 621	560 ± 316	0.66 ± 0.27
Median (min.–max.)	715 (431–3805)	647 (353–2353)	524 (61–1146)	0.70 (0.09–0.98)
No. of samples	10	10	10	10
		SE Asia Sector >7 km Altitude		
Mean ± SD	7000 ± 4586	5510 ± 3651	1815 ± 1914	0.31 ± 0.19
Median (min.–max.)	5041 (931–14802)	4196 (804–12245)	1129 (300–7689)	0.27 (0.07–0.68)
No. of samples	17	17	17	17

[a]Condensation nuclei units are #/cm^3 @ STP. No samples from the Channel sector at >7 km altitude or the WSW sector at <2 km altitude.

numbers above the heated CN columns are the mean percentages of nonvolatile (at 300°C) particles. What is striking here, is both the low mean values of total particles ($\approx$1000 cm^{-3}, along with the high percentage ($\geq$65%) of nonvolatile particles observed at midaltitudes (Figure 6) for all groups except NNW. This likely reflects the influence of cloud processing on these condensation nuclei. Clouds predominantly reside in this midaltitude (2–7 km) layer. Particles in this size range readily grow in clouds and volatile particles are scavenged. This has apparently led to preferential removal of these particles at midaltitudes.

3.6. Optical Properties

[35] Asian aerosols exert a great influence on the photochemistry of this region [*Lefer et al.*, 2003; *Tang et al.*, 2003a]. Aerosols influence photochemistry directly via their own scattering properties, and indirectly via their role in cloud formation, with cloud radiative properties also affecting photolysis rates. Photolysis frequencies are enhanced/reduced depending on whether the observation is above/below clouds and depending on whether the ambient aerosol population is highly scattering/absorbing [*Lefer et al.*, 2003]. While clouds have a greater instantaneous effect on photolysis frequencies [*Lefer et al.*, 2003], on average aerosols have a greater impact on O_3 production [*Tang et al.*, 2003a]. The net photochemical effect of clouds and aerosols during TRACE-P was a large decrease in photochemical O_3 in the boundary layer [*Lefer et al.*, 2003].

[36] The particulates in Asian megacity plumes can reduce NO_x photolysis such that the mixing ratio increases

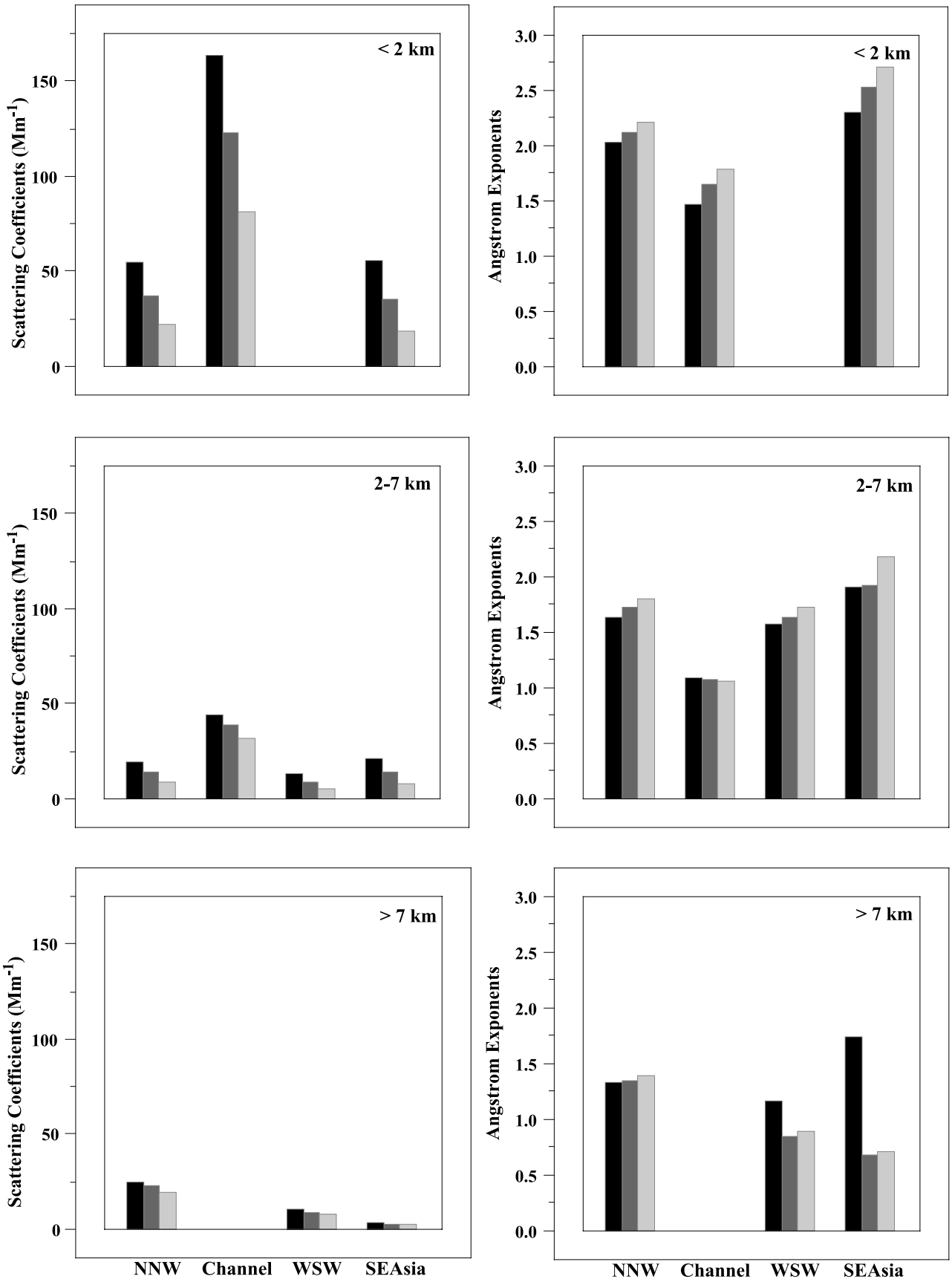

Figure 7. Mean scattering coefficients (left panels, 450 nm (black), 550 nm (medium gray), 700 nm (light gray)) and angstrom exponents (right panels, 450–700 nm (black), 450–550 nm (medium gray), 550–700 nm (light gray)) split by group and altitude.

Table 5. Single Scatter Albedo, Scattering Coefficients and Angstrom Exponent Means, Standard Deviations, Medians, Minima, and Maxima[a]

	ω_o	σ_{sp} 450 nm $\times 10^{-6}$ (m^{-1})	σ_{sp} 550 nm $\times 10^{-6}$ (m^{-1})	σ_{sp} 700 nm $\times 10^{-6}$ (m^{-1})	å 450–700	å 450–550	å 550–700
NNW Sector at <2 km Altitude							
Mean ± SD	0.87 ± 0.02	55 ± 21	37 ± 17	22 ± 13	2.03 ± 0.31	2.13 ± 0.26	2.21 ± 0.27
Median (min.–max.)	0.86 (0.81–0.93)	56 (10–123)	37 (7–112)	21 (4–90)	2.10 (0.77–2.40)	2.19 (1.31–2.48)	2.28 (1.27–2.54)
No. of samples	41	41	41	41	41	41	41
NNW Sector at 2–7 km Altitude							
Mean ± SD	0.84 ± 0.08	20 ± 23	14 ± 16	9 ± 10	1.64 ± 0.40	1.73 ± 0.46	1.80 ± 0.54
Median (min.–max.)	0.87 (0.65–0.94)	14 (4–121)	10 (3–82)	6 (3–48)	1.72 (0.81–2.37)	1.86 (0.34–2.35)	1.77 (0.31–2.69)
No. of samples	26	26	26	26	26	26	26
NNW Sector at >7 km Altitude							
Mean ± SD	0.93 ± 0.04	25 ± 24	23 ± 25	19 ± 23	1.33 ± 1.20	1.34 ± 0.74	1.40 ± 0.62
Median (min.–max.)	0.92 (0.88–0.98)	13 (6–70)	9 (3–67)	7 (2–59)	0.76 (0.0001–3.23)	1.43 (0.11–2.53)	1.24 (0.40–2.35)
No. of samples	8	10	10	10	10	10	10
Channel Sector at <2 km Altitude							
Mean ± SD	0.86 ± 0.02	163 ± 114	123 ± 86	82 ± 59	1.47 ± 0.48	1.65 ± 0.47	1.79 ± 0.47
Median (min.–max.)	0.85 (0.83–0.90)	97 (88–586)	71 (62–429)	45 (38–267)	1.63 (0.25–1.87)	1.80 (0.44–2.09)	1.94 (0.60–2.27)
No. of samples	25	23	23	23	23	23	23
Channel Sector at 2–7 km Altitude							
Mean ± SD	0.88 ± 0.05	44 ± 38	39 ± 36	31 ± 31	1.10 ± 0.54	1.08 ± 0.43	1.07 ± 0.37
Median (min.–max.)	0.87 (0.79–0.95)	31 (6–130)	26 (4–123)	21 (2–105)	1.01 (0.32–2.26)	0.97 (0.48–1.78)	1.01 (0.57–1.74)
No. of samples	13	13	13	13	13	13	13
WSW Sector at 2–7 km Altitude							
Mean ± SD	0.81 ± 0.08	13 ± 11	9 ± 7	6 ± 4	1.58 ± 1.07	1.64 ± 1.00	1.73 ± 0.83
Median (min.–max.)	0.82 (0.67–0.91)	11 (1–29)	7 (2–19)	5 (2–12)	1.98 (0.02–2.90)	2.02 (0.002–2.77)	1.77 (0.42–2.59)
No. of samples	7	7	7	7	7	7	7
WSW Sector at >7 km Altitude							
Mean ± SD	0.84 ± 0.08	10 ± 11	9 ± 9	8 ± 8	1.17 ± 0.95	0.85 ± 0.72	0.89 ± 0.60
Median (min.–max.)	0.86 (0.60–0.96)	6 (1–45)	5 (2–43)	5 (2–40)	1.19 (0.06–3.26)	0.59 (0.0001–2.37)	0.68 (0.06–2.36)
No. of samples	36	40	40	40	40	40	40
SE Asia Sector at <2 km Altitude							
Mean ± SD	0.82 ± 0.00	55 ± 4	35 ± 2	18 ± 1	2.30 ± 0.01	2.53 ± 0.002	2.72 ± 0.005
Median (min.–max.)	0.82 (0.82–0.82)	55 (53–58)	35 (33–37)	18 (17–19)	2.30 (2.29–2.31)	2.53 (2.53–2.53)	2.72 (2.72–2.72)
No. of samples	2	2	2	2	2	2	2
SE Asia Sector at 2–7 km Altitude							
Mean ± SD	0.78 ± 0.05	21 ± 16	14 ± 10	8 ± 6	1.91 ± 0.73	1.92 ± 0.76	2.17 ± 0.51
Median (min.–max.)	0.81 (0.71–0.84)	23 (1–43)	15 (1–30)	8 (1–19)	2.06 (0.05–2.58)	1.94 (0.11–2.79)	2.07 (1.54–2.94)
No. of samples	10	10	10	10	10	10	10
SE Asia Sector at >7 km Altitude							
Mean ± SD	0.80 ± 0.06	3 ± 1	2 ± 1	3 ± 1	1.75 ± 0.97	0.68 ± 0.59	0.70 ± 0.35
Median (min.–max.)	0.80 (0.71–0.90)	3 (0.5–6)	2 (2–4)	3 (1–4)	1.80 (0.0002–3.80)	0.47 (0.0001–2.06)	0.61 (0.27–1.49)
No. of samples	16	17	17	17	17	17	17

[a]No samples from the Channel sector at >7 km altitude or the WSW sector at <2 km altitude.

by 40% [*Tang et al.*, 2003a]. This is supported by the finding that HNO_3 and PAN dominate NO_y (NO_x < 100 pptv), except in plumes, where NO_x can be >1000 pptv [*Talbot et al.*, 2003]. O_3 is produced by the photolysis of NO_2. Hence, reducing NO_x photolysis, reduces O_3 production. Since the photolysis of O_3 produces OH and OH is the primary sink of CO, it is also expected that the aerosol influence on photolysis will reduce O_3 and increase CO in plumes [*Tang et al.*, 2003a]. This is supported by observations made during PHOBEA-II (flight 8, April 14, 2001), where an Asian dust plume transported to North America was found to have O_3 anti-correlated with aerosol scattering [*Price et al.*, 2003]. Further, the highest CO observed during PHOBEA-II was associated with this plume [*Price et al.*, 2003].

[37] To accurately model photochemistry then, a good understanding of aerosol optical properties is needed for any given region. In the next three sub-sections, we will discuss the scattering coefficients, angstrom exponents, and single scatter albedo measurements in the same context as we did for the chemical and size distribution data.

3.6.1. Scattering

[38] The scattering coefficients (σ_{sp}) obtained from an integrating nephelometer as a function of group and altitude, show Channel enhanced compared to the other groups both at low and midaltitudes (left panels Figure 7; Table 5). Otherwise, at each altitude level, mean σ_{sp} is not statistically significantly different between the groups. Submicron particles are the most efficient scatterers, particularly in the 0.2–1.0 μm diameter range [*Quinn et al.*, 2002a]. Further,

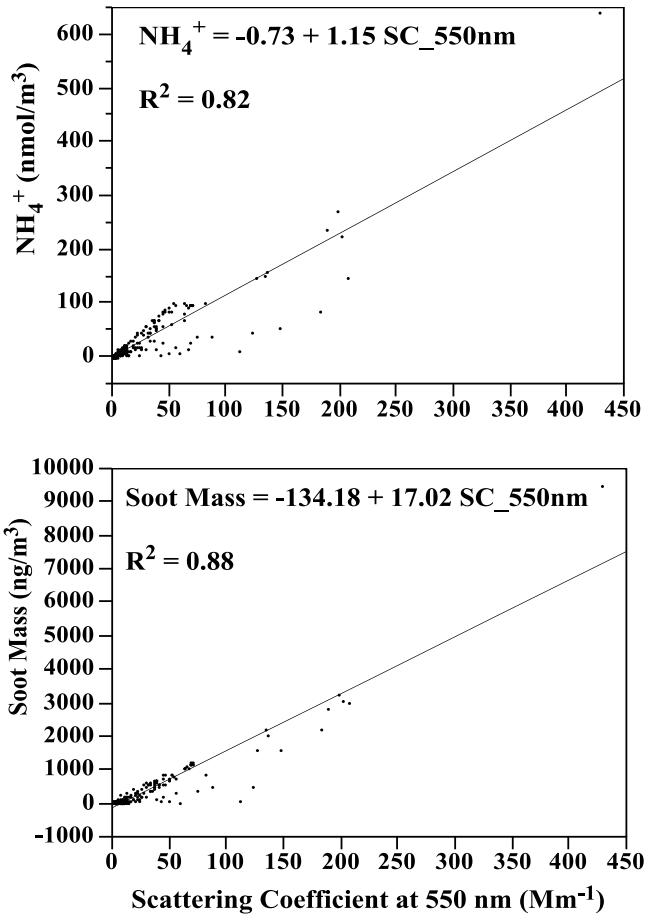

Figure 8. NH_4^+ mixing ratio and soot mass plotted versus the scattering coefficient for 550 nm.

σ_{sp} is mostly strongly dependent upon the amount of particulate matter present, as opposed to its size distribution or composition [*Delene and Ogren*, 2002]. Note that good correlations are found for both NH_4^+ (R^2 = 0.82) and soot (R^2 = 0.88) versus σ_{sp}(550 nm) (Figure 8). These overall correlations are driven primarily by the Channel and SE Asia sectors, with R^2 = 0.83 and 0.94, respectively for NH_4^+ and R^2 = 0.90 and 0.93 for soot. The other two sectors have much poorer correlations of 0.40 (NNW NH_4^+), 0.25 (WSW NH_4^+), 0.42 (NNW soot), and 0.20 (WSW soot). It seems likely the good correlations observed for the Channel and SE Asia sectors are due to the prevalence of fine mode particulates in these regions.

[39] Channel, with the most fine mode particles (see section 3.3, Figure 5), exhibits the highest values of σ_{sp} (e.g., 123 and 39 Mm^{-1} at 550 nm for low and midaltitude samples, respectively). Comparable values of σ_{sp} observed in NNW and SE Asia at low altitudes ($\approx$35 Mm^{-1} at 550 nm) reflect the comparable numbers of particles present (Figure 5 top left panel). Lower σ_{sp} observed, <10 Mm^{-1} at 550 nm, for WSW and high altitude SE Asia is consistent with the lower number densities observed in these sectors at their respective altitudes, compared to the other groups (Figures 5 and 7; Table 5). These values are consistent with those reported by *Quinn et al.* [2002b] for their eight source regions during INDOEX, with median values ranging from about 15–135 Mm^{-1} at 550 nm. Similarly, *Sheridan et al.* [2002] reported a mean value of 53 Mm^{-1} at 550 nm observed on the C-130 during INDOEX.

3.6.2. Angstrom Exponent

[40] Although, we measured size distributions directly (see section 3.3) with PCASP and FSSP probes, an underlying goal of the Global Troposphere Experiments has been to link in situ measurements with satellite observations [*Crawford et al.*, 2003]. The angstrom exponent is a measure of the wavelength dependence of scattering which can be used to describe aerosol size information based on a remotely sensed measurement [*Price et al.*, 2003]. Hence, in this section, we describe the angstrom exponents measured by the DC-8 in comparison with the measured size distributions, although this is somewhat redundant with the information presented in section 3.3. In principle, space-based observations of angstrom exponents may eventually provide regional- and global-scale inputs of aerosol size distributions for regional and global models.

[41] The angstrom exponent (å) decreases with increasing particle size, from values of 3 to 1 between 10 and 1000 nm. For particle distributions dominated by supermicron particles, å approaches 0 [*Price et al.*, 2003]. Comparing the mean å shown in Figure 7 (right panels) to the volume distributions shown in Figure 5 (right panels), å clearly reflects the presence of larger particles. The greatest influence of the larger particles is seen in low altitude Channel (due to the presence of dust), followed by NNW (due to sea salt), with the highest values observed in SE Asia at these altitudes.

[42] Note, å is calculated from the scattering coefficients [*Delene and Ogren*, 2002], which most strongly respond to particles in the 0.2–1.0 μm diameter range [*Quinn et al.*, 2002a]. So the shifting size distributions indicated by å most strongly reflect this submicron mode rather than the supermicron sizes where the bulk of the dust and sea salt mass resides. Due to inefficiencies with the nephelometer inlet on the DC-8, supermicron particles were not passed efficiently through to the instrument. This is a greater problem for the sea salt particles than the dust particles. However, since the submicron fraction dominates the scattering, it is not expected that the scattering coefficients and angstrom exponents reported here are greatly affected by the inlet problems.

[43] Observations of Asian dust transported to the eastern Pacific/western United States made during PHOBEA-II flight 8 showed å of 0.6 (450/550) and 0.8 (550/700) in the heaviest dust layers [*Price et al.*, 2003]. These values are comparable to the lowest values measured in Channel by the DC-8 during TRACE-P of $\approx$0.5 (450/550, Table 5) and $\approx$0.6 (550/700, Table 5). The nephelometer used during PHOBEA-II also did not pass supermicron particles efficiently [*Price et al.*, 2003], so the different values here probably reflect a somewhat larger size distribution near Asia.

[44] Mean angstrom exponents reported by *Quinn et al.* [2002b] during INDOEX range from <0.25 to about 1.7 (for 450–700 nm) for the 8 sources regions they observed. These values are lower than the mean values reported here for SE Asia and WSW (1.17–2.30, 450–700 nm). This reflects the larger particles included in their measurement (up to 10 μm) compared to those here (up to 1 μm). *Sheridan et al.* [2002] report a mean value of 2.02 (550–

700 nm) measured on the C-130 during INDOEX, with mean values from their most polluted region ranging from 1.37 (>5 km) to about 2.0 at lower altitudes. These values are for submicron particles only, so are more comparable to those measured here in SE Asia and WSW. However, they span a narrower range of values than these two groups, 0.70–2.72 (550–700 nm) for SE Asia and 0.89–1.73 (550–700 nm) for WSW.

3.6.3. Single Scatter Albedo

[45] Single scatter albedo (ω_o) indicates the relative proportion of scattering and absorbing coefficients [$\sigma_{sp}/(\sigma_{sp} + \sigma_{ap})$] such that a greater relative presence of absorbing soot compared to sulfate will result in a lower ω_o [*Delene and Ogren*, 2002]. While the greatest amount of soot was observed in Channel, the greatest amount of sulfate was observed there as well. Thus, the mean ω_o in Channel is not the lowest observed (Table 5). The lowest mean ω_o is seen in SE Asia (Table 5), where the relative proportion of soot particulates is much higher than in any other group (see Table 3). Most of the SE Asia means ($\approx$0.80) are statistically significantly lower than those of the other groups ($\approx$0.84–0.93), while the means of the other groups are not significantly different from each other. The lowest values measured were in the WSW group ($\approx$0.60, Table 5). These observations for WSW and SE Asia are consistent with those of *Sheridan et al.* [2002], who found mean values of $\omega_o \approx 0.80$ for their most polluted sector at altitudes above 3 km during INDOEX.

[46] If the soot and sulfate present in SE Asia and WSW are externally mixed, the mean ω_o indicates ammonium sulfate dominates the mixture (constituting about 80% of the mass [*Seinfeld and Pandis*, 1998]). If however, these constituents are internally mixed, e.g., a soot core, with a sulfate coating, then these materials each contribute about 50% by mass to the mixture on average. An aerosol population for these regions consisting of approximately 80% sulfate and 20% soot is consistent with the findings of *Bush and Valero* [2002], who found during INDOEX that an aerosol mixture with 83% from highly scattering sulfate-type aerosols and 17% from absorptive soot-type aerosols could best explain the total aerosol optical depth at 500 nm. Further, they found similar contributions whether the observation was made on days with relatively low or high aerosol concentrations, suggesting the composition remains consistent, despite differences in total aerosol concentrations. In the NNW and Channel sectors, which exhibit larger mean ω_o, sulfate dominates the mixture whether it is internally or externally mixed.

4. Summary

[47] We have presented the chemical and physical aerosol data obtained on the DC-8 platform during TRACE-P, grouped based on back trajectories into four sectors and divided into three altitude levels. The four sectors represent long range transport from the west (WSW), regional circulation over the western Pacific and Southeast Asia (SE Asia), polluted transport from northern Asia with substantial sea salt at low altitudes (NNW) and a substantial amount of dust (Channel).

[48] The highest mean mixing ratios of water-soluble ions and soot were observed at the lowest altitudes (<2 km) in the Channel sector, with 217 nmol/m^3 Ca^{2+}, 148 nmol/m^3 NH_4^+, 129 nmol/m^3 $SO_4^=$, 108 nmol/m^3 NO_3^-, and 2201 ng/m^3 soot. NNW had the highest mean sea salt mixing ratios, 105 nmol/m^3 Na^+ and 104 nmol/m^3 Cl^-, while NH_4^+ and $SO_4^=$ were about a factor of 2 lower than those in low altitude Channel and Ca^{2+} was an order of magnitude lower (14 nmol/m^3). Low altitude SE Asia had lower mixing ratios in general, with Na^+, Cl^-, and Ca^{2+} < 10 nmol/m^3 and NH_4^+ and $SO_4^=$ about 30 nmol/m^3. However, soot is relatively important in this region, contributing 638 ng/m^3 in the low altitude samples and 219 ng/m^3 in the midaltitude samples on average. WSW has generally low mixing ratios at both middle and high altitudes, with no species >10 nmol/m^3 and <100 ng/m^3 of soot.

[49] The bulk of the aerosol mass (determined from soot, sea salt, dust, and water-soluble inorganic ions, no organic species included here) exported from Asia emanates from Channel below 2 km altitude, 134 μg/m^3 on average, compared with 50 μg/m^3 at these altitudes from NNW. Between 2 and 7 km, Channel still exports the most particulate material, averaging 50 μg/m^3 compared with 7, 4, and 3 μg/m^3 from NNW, SE Asia, and WSW, respectively. At high altitudes <4 μg/m^3 is exported on average, from all sectors.

[50] Dust contributes 79% of the mass in the Channel sector, followed by non-sea-salt water-soluble inorganic species (17%) below 2 km. At these altitudes, NNW aerosol has comparable amounts of sea salt, dust, and non-sea-salts, 33%, 28%, and 36%, respectively. The bulk of the mass for both SE Asia and WSW is due to non-sea-salt water-soluble inorganic species, although SE Asia also contains a relatively high proportion of soot, 12% at low altitudes, 7% between 2 and 7 km.

[51] The aerosol physical data is consistent with the chemical data. Number density and volume distributions support the chemical data showing enhanced fine particles in Channel and NNW as well as enhanced supermicron volumes for these sectors due to sea salt and dust. The highest condensation nuclei number densities are in the Channel sector at low altitudes, with ultrafine particles >4 nm exceeding 17,000 particles/cm^3 on average. At midaltitudes (2–7 km) mean condensation nuclei number densities are at their lowest ($\approx$1000 particles cm^{-3}), while the nonvolatile fraction is at its highest (51% NNW, $\geq$65% for the other groups). This is attributed to wet scavenging which removes hygroscopic CN particles.

[52] Enhanced scattering (>80 Mm^{-1}) in the Channel sector is attributed to the high densities of fine particles compared to other groups. Angstrom exponents show good agreement with the volume measurements, yielding the lowest mean values in the dusty Channel sector. The single scatter albedo reflects the enhanced soot in the SE Asia sector, with mean values of about 0.80. The polluted sectors, NNW and Channel have means ranging from 0.84–0.93.

[53] The industrialization of Asia is expected to continue, leading to an increase in emissions of both gases and particulates. Throughout this TRACE-P special section, aerosols are shown to play various important roles in the composition and evolution of Asian outflow. Aerosols exhibit extreme spatial and temporal heterogeneity complicating their representation in regional and global models.

This overview has tried to provide a context for better understanding the composition, physical properties, and distribution of aerosols measured during TRACE-P, and their role in the export and evolution of Asian continental outflow.

[54] **Acknowledgments.** The authors are grateful for the extensive assistance provided by John Holdzkom and Sarah Bittenbender for the 3-D visualization of the back trajectories in vGeo. The authors also wish to thank the NASA Global Tropospheric Chemistry Program and the National Research Council for their support of this work.

References

Anderson, T. L., et al., Performance characteristics of a high-sensitivity, three wavelength, total scatter/backscatter nephelometers, *J. Atmos. Oceanic Technol.*, *13*, 967–986, 1996.

Bates, T. S., D. J. Coffman, D. S. Covert, and P. K. Quinn, Regional marine boundary layer aerosol size distributions in the Indian, Atlantic, and Pacific Oceans: A comparison of INDOEX measurements with ACE-1, ACE-2, and Aerosols99, *J. Geophys. Res.*, *107*(D19), 8026, doi:10.1029/2001JD001174, 2002.

Blake, N., et al., NMHCs and halocarbons in Asian continental outflow during Transport and Chemical Evolution Over the Pacific (TRACE-P): Comparison With PEM-West B, *J. Geophys. Res.*, *108*(D20), 8806, doi:10.1029/2002JD003367, 2003.

Bodhaine, B. A., et al., Three-wavelength nephelometer suitable for aircraft measurement of background aerosol scattering coefficient, *Atmos. Environ.*, *25A*, 2267–2276, 1991.

Bond, C. T., et al., Calibration and intercomparison of filter-based measurements of visible light absorption by aerosols, *Aerosol Sci. Technol.*, *30*, 582–600, 1999.

Bush, B. C., and F. P. J. Valero, Spectral aerosol radiative forcing at the surface during the Indian Ocean Experiment (INDOEX), *J. Geophys. Res.*, *107*(D19), 8003, doi:10.1029/2000JD000020, 2002.

Charlson, R. J., et al., Climate forcing by anthropogenic aerosols, *Science*, *255*, 423–430, 1992.

Crawford, J., et al., Clouds and trace gas distributions during TRACE-P, *J. Geophys. Res.*, *108*(D21), 8818, doi:10.1029/2002JD003177, in press, 2003.

Delene, D. J., and J. A. Ogren, Variability of aerosol optical properties at four North American surface monitoring sites, *J. Atmos. Sci.*, *59*, 1135–1150, 2002.

Dibb, J. E., R. W. Talbot, E. M. Scheuer, D. R. Blake, N. J. Blake, G. L. Gregory, G. W. Sachse, and D. C. Thornton, Aerosol chemical composition and distribution during the Pacific Exploratory Mission, Tropics, *J. Geophys. Res.*, *104*, 5785–5800, 1999.

Dibb, J. E., R. W. Talbot, and E. M. Scheuer, Composition and distribution of aerosols over the North Atlantic during the Subsonic Assessment Ozone and Nitrogen Oxide Experiment (SONEX), *J. Geophys. Res.*, *105*, 3709–3717, 2000.

Dibb, J. E., R. W. Talbot, G. Seid, C. Jordan, E. Scheuer, E. Atlas, N. J. Blake, and D. R. Blake, Airborne sampling of aerosol particles: Comparison between surface sampling at Christmas Island and P-3 sampling during PEM-Tropics B, *J. Geophys. Res.*, *107*, 8230, doi:10.1029/2001JD000408, 2002. [printed *108*(D2), 2003]

Dibb, J. E., R. W. Talbot, E. Scheuer, G. Seid, M. Avery, and H. Singh, Aerosol chemical composition in Asian continental outflow during the Transport and Chemical Evolution Over the Pacific (TRACE-P): Comparison with PEM-West B, *J. Geophys. Res.*, *108*(D21), 8815, doi:10.1029/2002JD003111, in press, 2003.

Fuelberg, H. E., R. O. Loring Jr., M. V. Watson, M. C. Sinha, K. E. Pickering, A. M. Thompson, G. W. Sachse, D. R. Blake, and M. R. Schoeberl, TRACE-A Trajectory Intercomparison: 2. Isentropic and kinematic methods, *J. Geophys. Res.*, *101*, 23,927–23,939, 1996.

Fuelberg, H. E., R. E. Newell, S. P. Longmore, W. Zhu, D. J. Westberg, E. V. Browell, D. R. Blake, G. L. Gregory, and G. W. Sachse, A meteorological overview of the PEM-Tropics period, *J. Geophys. Res.*, *104*, 5585–5622, 1999.

Fuelberg, H. E., J. R. Hannan, P. F. J. van Velthoven, E. V. Browell, G. Bieberbach Jr., R. D. Knabb, G. L. Gregory, K. E. Pickering, and H. B. Selkirk, A meteorological overview of the SONEX period, *J. Geophys. Res.*, *105*, 3633–3651, 2000.

Fuelberg, H. E., C. M. Kiley, J. R. Hannan, D. J. Westberg, M. A. Avery, and R. E. Newell, Meteorological conditions and transport pathways during the Transport and Chemical Evolution over the Pacific (TRACE-P) experiment, *J. Geophys. Res.*, *108*(D20), 8782, doi:10.1029/2002JD003092, 2003.

Hasegawa, S., and S. Ohta, Some measurements of the mixing state of soot containing particles at urban and non-urban sites, *Atmos. Environ.*, *36*, 3899–3908, 2002.

Heald, C., D. J. Jacob, P. I. Palmer, M. J. Evans, G. W. Sachse, H. B. Singh, and D. R. Blake, Biomass burning emission inventory with daily resolution: Application to aircraft observations of Asian outflow, *J. Geophys. Res.*, *108*(D21), 8811, doi:10.1029/2002JD003082, in press, 2003.

Huebert, B. J., T. Bates, P. B. Russell, G. Shi, Y. J. Kim, K. Kawamura, G. Carmichael, and T. Nakajima, An overview of ACE-Asia: Strategies for quantifying the relationships between Asian aerosols and their climatic impacts, *J. Geophys. Res.*, *108*(DXX), doi:10.1029/2003JD003550, in press, 2003.

Jacob, D. J., J. H. Crawford, M. M. Kleb, V. S. Connors, R. J. Bendura, J. L. Raper, G. W. Sachse, J. C. Gille, L. Emmons, and C. L. Heald, Transport and Chemical Evolution Over the Pacific (TRACE-P) mission: Design, execution, and first results, *J. Geophys. Res.*, *108*(D20), 9000, doi:10.1029/2002JD003276, 2003.

Jordan, C. E., J. E. Dibb, B. E. Anderson, and H. E. Fuelberg, Uptake of nitrate and sulfate on dust aerosols during TRACE-P, *J. Geophys. Res.*, *108*(D21), 8817, doi:10.1029/2002JD003101, 2003.

Kahl, J. D., A cautionary note on the use of air trajectories in interpreting atmospheric chemistry measurements, *Atmos. Environ.*, *27A*, 3037–3038, 1993.

Kasten, F., Visibility forecast in the phase of pre-condensation, *Tellus*, *21*(5), 631–635, 1969.

Lefer, B., R. E. Shetter, S. R. Hall, J. H. Crawford, and J. R. Olson, Impact of clouds and aerosols on photolysis frequencies and photochemistry during TRACE-P: 1. Analysis using radiative transfer and photochemical box models, *J. Geophys. Res.*, *108*(D21), 8821, doi:10.1029/2002JD003171, in press, 2003.

Li, Q., D. J. Jacob, R. M. Yantosca, C. L. Heald, H. Singh, M. Koike, Y. Zhao, G. W. Sachse, and D. Streets, A global three-dimensional model analysis of the atmospheric budgets of HCN and CH_3CN: Constraints from aircraft and ground measurements, *J. Geophys. Res.*, *108*(D21), 8827, doi:10.1029/2002JD003075, 2003.

Liu, H., D. J. Jacob, I. Bey, R. M. Yantosca, B. N. Duncan, and G. W. Sachse, Transport pathways for Asian combustion outflow over the Pacific: Interannual and seasonal variations, *J. Geophys. Res.*, *108*(D20), 8786, doi:10.1029/2002JD003102, 2003.

Ma, Y., et al., Characteristics and influence of biosmoke on the fine-particle ionic composition measured in Asian outflow during the Transport and Chemical Evolution Over the Pacific (TRACE-P) experiment, *J. Geophys. Res.*, *108*(D21), 8816, doi:10.1029/2002JD003128, in press, 2003.

Maloney, J. C., H. E. Fuelberg, M. A. Avery, J. H. Crawford, D. R. Blake, B. G. Heikes, G. W. Sachse, S. T. Sandholm, H. Singh, and R. W. Talbot, Chemical characteristics of air from different source regions during the second Pacific Exploratory Mission in the Tropics (PEM-Tropics B), *J. Geophys. Res.*, *106*, 32,609–32,625, 2001.

Mayol-Bracero, O. L., R. Gabriel, M. O. Andreae, T. W. Kirchstetter, T. Novakov, J. Ogren, P. Sheridan, and D. G. Streets, Carbonaceous aerosols over the Indian Ocean during the Indian Ocean Experiment (INDOEX): Chemical characterization, optical properties, and probable sources, *J. Geophys. Res.*, *107*(D19), 8030, doi:10.1029/2000JD000039, 2002.

Price, H. U., D. A. Jaffe, P. V. Doskey, I. McKendry, and T. Anderson, Vertical profiles of O_3, aerosols, CO and NMHCs in the northeast Pacific during the TRACE-P and ACE-ASIA experiments, *J. Geophys. Res.*, *108*(D20), 8799, doi:10.1029/2002JD002930, 2003.

Quinn, P. K., T. L. Miller, T. S. Bates, J. A. Ogren, E. Andrews, and G. E. Shaw, A 3-year record of simultaneously measured aerosol chemical and optical properties at Barrow, Alaska, *J. Geophys. Res.*, *107*(D11), 4130, doi:10.1029/2001JD001248, 2002a.

Quinn, P. K., D. J. Coffman, T. S. Bates, T. L. Miller, J. E. Johnson, E. J. Welton, C. Neusüss, M. Miller, and P. J. Sheridan, Aerosol optical properties during INDOEX 1999: Means, variability, and controlling factors, *J. Geophys. Res.*, *107*(D19), 8020, doi:10.1029/2000JD000037, 2002b.

Russo, R., et al., Chemical composition of Asian continental outflow over the western Pacific: Results from Transport and Chemical Evolution over the Pacific (TRACE-P), *J. Geophys. Res.*, *108*(D20), 8804, doi:10.1029/2002JD003184, 2003.

Seinfeld, J. H., and S. N. Pandis, *Atmospheric Chemistry and Physics*: *From Air Pollution to Climate Change*, John Wiley, Hoboken, N. J., 1998.

Sheridan, P. J., A. Jefferson, and J. A. Ogren, Spatial variability of submicrometer aerosol radiative properties over the Indian Ocean during INDOEX, *J. Geophys. Res.*, *107*(D19), 8011, doi:10.1029/2000JD000166, 2002.

Singh, H. B., et al., In situ measurements of HCN and CH_3CN over the Pacific Ocean: Sources, sinks, and budgets, *J. Geophys. Res.*, *108*(D20), 8795, doi:10.1029/2002JD003006, 2003.

Song, C. H., and G. R. Carmichael, Gas-particle partitioning of nitric acid modulated by alkaline aerosol, *J. Atmos. Chem.*, *40*, 1–22, 2001.

Stohl, A., Computation, accuracy, and applications of trajectories—A review and bibliography, *Atmos. Environ.*, *32*, 947–966, 1998.

Stohl, A., G. Wotawa, P. Seibert, and H. Kromp-Kolb, Interpolation errors in wind fields as a function of spatial and temporal resolution and their impact on different types of kinematic trajectories, *J. Appl. Meteorol.*, *34*, 2149–2165, 1995.

Streets, D., et al., An inventory of gaseous and primary aerosol emissions in Asia in the year 2000, *J. Geophys. Res.*, *108*(D21), 8809, doi:10.1029/2002JD003093, in press, 2003.

Sun, J., M. Zhang, and L. Tungsheng, Spatial and temporal characteristics of dust storms in China and its surrounding regions, 1960–1999: Relations to source area and climate, *J. Geophys. Res.*, *106*, 10,325–10,333, 2001.

Talbot, R., et al., Reactive nitrogen in Asian continental outflow over the western Pacific: Results from the NASA TRACE-P airborne mission, *J. Geophys. Res.*, *108*(D20), 8803, doi:10.1029/2002JD003129, 2003.

Tang, Y., et al., Impacts of aerosols and clouds on photolysis frequencies and photochemistry during TRACE-P: 2. Three-dimensional study using a regional chemical transport model, *J. Geophys. Res.*, *108*(D21), 8822, doi:10.1029/2002JD003100, in press, 2003a.

Tang, Y., et al., Influences of biomass burning during the Transport and Chemical Evolution Over the Pacific (TRACE-P) experiment identified by the regional chemical transport model, *J. Geophys. Res.*, *108*(D21), 8824, doi:10.1029/2002JD003110, in press, 2003b.

B. E. Anderson and C. H. Hudgins, Atmospheric Sciences Competency, NASA Langley Research Center, MS 483, Hampton, VA 23681, USA. (b.e.anderson@larc.nasa.gov)

J. E. Dibb and R. Russo, Climate Change Research Center, Institute for the Study of Earth, Oceans, and Space, University of New Hampshire, Durham, NH 03824, USA.

H. E. Fuelberg and C. M. Kiley, Department of Meteorology, Florida State University, Tallahassee, FL 32306, USA.

C. E. Jordan, National Research Council, NASA Langley Research Center, MS 483, Hampton, VA 23681, USA. (c.e.jordan@larc.nasa.gov)

E. Scheuer, G. Seid, and R. W. Talbot, Complex Systems Research Center, Institute for the Study of Earth, Oceans, and Space, University of New Hampshire, Durham, NH 03824, USA.

K. L. Thornhill, SAIC, NASA Langley Research Center, MS 483, Hampton, VA 23681, USA.

E. Winstead, GATS, NASA Langley Research Center, MS 483, Hampton, VA 23681, USA.

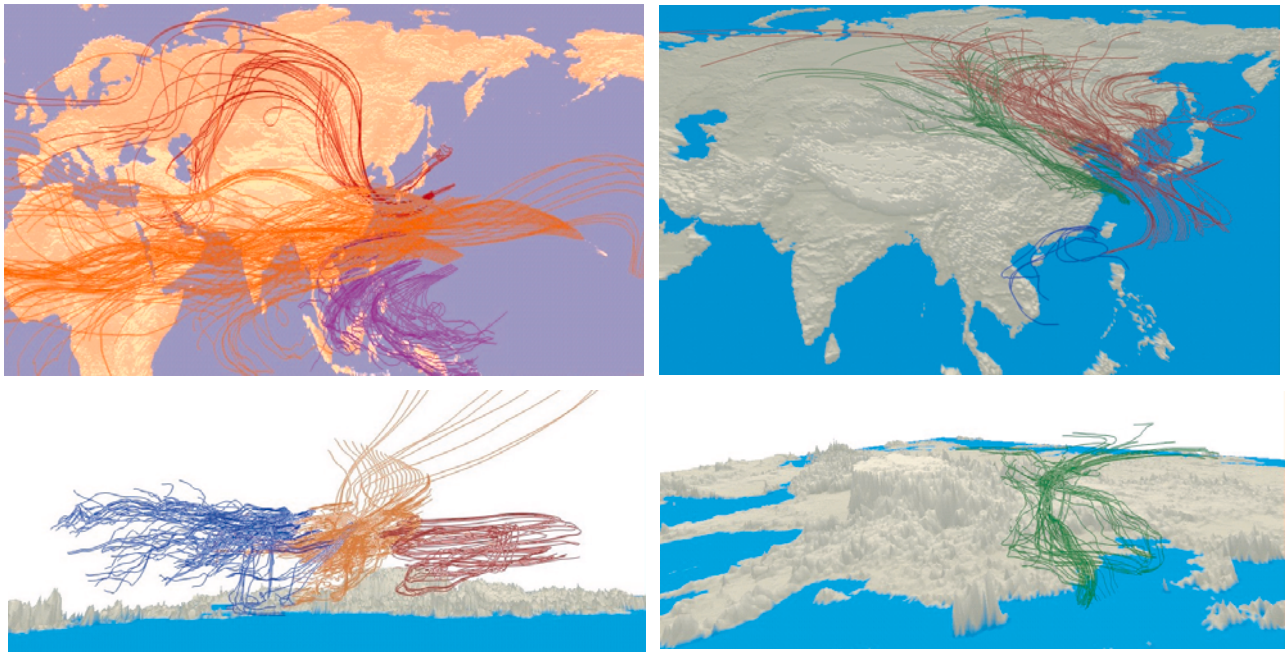

Figure 1. Back trajectories for the aerosol samples divided into four sectors. The top left panel shows trajectories for samples collected at altitudes >7 km. Only three sectors are represented at those altitudes, NNW (red), WSW (gold), and SE Asia (blue). The bottom left panel is a side view from the Pacific Ocean looking toward the Tibetan Plateau. This view shows these trajectories typically represent high altitude long distance transport. The top right panel shows trajectories for samples collected at altitudes <2 km. Only three sectors are represented at these altitudes, NNW (red), Channel (green), and SE Asia (blue). The bottom right panel shows only the low altitude Channel trajectories, angled to show that these trajectories flow along the surface and are confined by the surface topography.

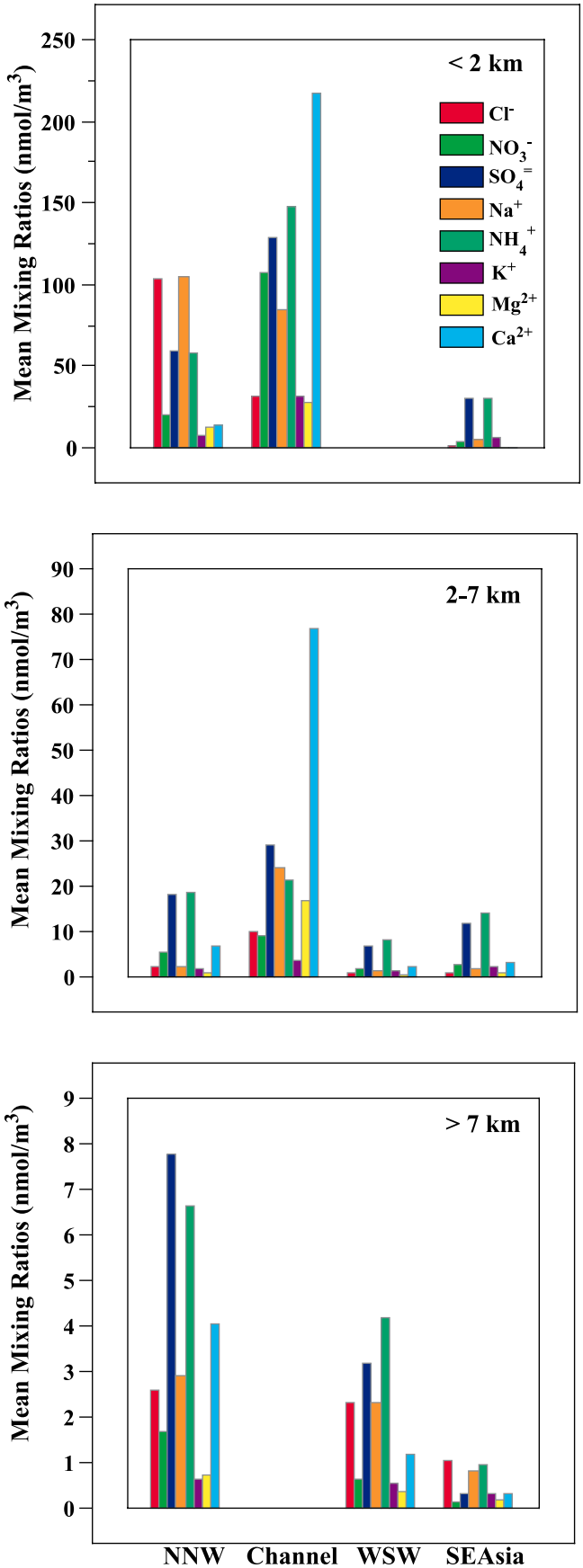

Figure 2. Aerosol mean chemical signatures for each group, split by altitude.